Electrophysiological Mechanisms in the Anterior Insula Cortex during Reward Expectancy

Linglin Yang[1,2], Katia Lehongre[3], Hongyi Ye[2], XinFeng Yu[4], Vincent Navarro[5,6,7], Sen Cheng[8], Zheng Lin[1], Nikolai Axmacher[9,10], Shuang Wang[2,*], Hui Zhang[9,*]

[1] Department of Psychiatry, Second Affiliated Hospital, School of medicine, Zhejiang University, 310020 Hangzhou, China

[2] Department of Neurology, Epilepsy center, Second Affiliated Hospital, School of medicine, Zhejiang University, 310020 Hangzhou, China

[3] CENIR - Centre de Neuro-Imagerie de Recherche, Paris Brain Institute, ICM, Hôpital de la Pitié-Salpêtrière, 75013 Paris, France

[4] Department of Radiology, Second Affiliated Hospital, School of medicine, Zhejiang University, 310020 Hangzhou, China

[5] Sorbonne Université, Inserm, CNRS, Paris Brain Institute, ICM, Hôpital de la Pitié-Salpêtrière, 75013 Paris, France

[6] Epilepsy Unit, AP-HP, PitiéSalpêtrière Hospital, 75013 Paris, France

[7] Clinical Neurophysiology Department, AP-HP, Pitié-Salpêtrière Hospital, 75013 Paris, France

[8] Institute for Neural Computation, Faculty of Computer Science, Ruhr University Bochum, 44801 Bochum, Germany

[9] Department of Neuropsychology, Institute of Cognitive Neuroscience, Faculty of Psychology, Ruhr University Bochum, 44801 Bochum, Germany

[10] State Key Laboratory of Cognitive Neuroscience and Learning and IDG/McGovern Institute for Brain Research, Beijing Normal University, 100875 Beijing, PR China

* Correspondence
Hui.Zhang-c5u@ruhr-uni-bochum.de (Hui Zhang)
wangs77@zju.edu.cn (Shuang Wang)

Abstract

Reward expectancy contributes to behavioral performance by coordinating the allocation of cognitive resources, which incorporates the involvement of the anterior insular cortex (AIC). To investigate the electrophysiological mechanisms underlying reward expectancy in the AIC, we collected intracranial electroencephalography (iEEG) data from epilepsy patients implanted for clinical purposes. During the recording, they navigated a virtual T-maze where they encountered rewards at three predetermined locations. We focused on the time window proximal to entering the reward zone, which was defined as the expectancy stage. During this stage, a strong phase-amplitude coupling (PAC) effect was found between local theta oscillation and gamma activity within the AIC. Interestingly, the PAC effect exhibited a specific temporal structure in which the peak gamma power was progressively coupled to an earlier theta phase before each onset of the same reward. Meanwhile, the reward-specific brain patterns were pre-activated during the expectancy stage of rewards. This pre-activation was tended to take place simultaneously with the occurrence of peak gamma activities across individual trials. Furthermore, the pre-activation of reward-specific patterns also progressively shifted forward on theta phases as more trials were conducted. These phenomena of phase shift were reminiscent of the phase precession effect in which single neurons fire at progressively earlier phases of low-frequency oscillations, and thus were called phase-precession-like effects (PPLEs). Additionally, subjects exhibiting PPLEs in the AIC presented less variability and a more notable improvement in response latency across trials. These results revealed possible electrophysiological mechanisms of the AIC underlying reward expectancy.

Keywords:

anterior insular cortex; reward expectancy; temporal structure; phase-precession-like effect; phase-amplitude coupling; reward-specific neural pattern; intracranial electroencephalography

Introduction

Many daily behaviors of humans are driven by the expectancy of rewards, whether material or spiritual (Pessiglione et al., 2007; Rowe et al., 2008). Reward expectancy has been proposed to boost behavioral performance (Rowe et al., 2008), particularly when the expected reward is ultimately obtained (Bein et al., 2023; Frömer et al., 2021). Typically, representations of rewards are tightly linked to various stimuli, such as spatial contexts, establishing associations between reward and context (Blaukopf & DiGirolamo, 2007). When a reward-associated context is recognized, it will trigger the activation of neural patterns for the reward based on the memory (Bein et al., 2023). It subsequently promotes our brain to allocate more cognitive resources, such as attention and motivation, to scan for the expected reward in the matched context (Baruni et al., 2015; Bein et al., 2023; Frömer et al., 2021; Rowe et al., 2008). The emergence of a reward consistent with expectation will in turn enhance the context-reward association by strengthening the reward-related representation (Bein et al., 2023; Bergmann et al., 2019; Grill-Spector et al., 2006). Collectively, the process of reward expectancy includes information integration, salience identification, and attention allocation (Bein et al., 2023). Of note, all of them incorporate the involvement of the salience network (Seeley et al., 2007). As a critical component of the salience network, the anterior insula cortex (AIC) activates ahead of other cortical areas during various cognitive tasks, such as the oddball attention task (Sridharan et al., 2008) and flanker task (Cai et al., 2016). These preceding neural activities in the AIC are speculated to participate in integrating information and allocating cognitive resources (Dajani & Uddin, 2015; Molnar-Szakacs & Uddin, 2022), thereby involved in reward expectancy (Rothkirch et al., 2014). Recently, electrophysiological study in monkeys has revealed neuronal activities related to reward expectancy in the AIC, showing that approximately a quarter of responsive neurons are activated prior to an expected reward (Mizuhiki et al., 2012). Nevertheless, the exact electrophysiological mechanism of the AIC in reward expectancy is poorly understood. Exploring the reward expectancy related activities in the AIC might shed light on promoting information processing speed and working efficiency.

Intracranial electroencephalography (iEEG) provides abundant information that unveils the rapid brain dynamics during cognitive processes in deep brain regions (e.g., the AIC). It is noteworthy that prominent gamma activities emerge at specific phases of theta oscillations, a phenomenon known as phase-amplitude coupling (PAC) (Axmacher et al., 2010; Canolty & Knight, 2010; Tort et al., 2009). The mechanism offers an effective means for inter-regional information transfer because slower theta oscillations spread to wider areas and synchronize local gamma generators in individual brain regions (González et al., 2020; Lisman, 2005; McGinn & Valiante, 2014). A strengthened PAC effect facilitates information integration in the brain (Canolty & Knight, 2010; Mariscal, Levin, et al., 2021), boosts memory formation (Axmacher et al., 2010), and helps to establish the relationship between context and items (Tort et al., 2009; Zheng et al., 2022). These studies highlight the significance of PAC in the context of reward expectancy and its role in integrating information.

Moreover, basic characteristics of PAC may reflect the functional configuration of a neural network during a given task. Phases of low-frequency oscillations, corresponding to the peak of high-frequency activities, represent distinct neural signatures implicated in a range of cognitive tasks (Bush & Burgess, 2020; Lopour et al., 2013). For example, gamma activities coupled to the peak of theta oscillations contribute to memory encoding, while those coupled to the trough of theta oscillations participate in memory retrieval (Kragel et al., 2020; Lopes-Dos-Santos et al., 2018; Rayan et al., 2022). When encoding sequential events, the neural pattern underlying each event is associated with different phases of low-frequency oscillations in the frontal and temporal lobes (Axmacher et al., 2010; Bahramisharif et al., 2018; Heusser et al., 2016; Lisman, 2005; Reddy et al., 2021; Siegel et al., 2009; Watrous et al., 2015; Yang et al., 2021). Such a phase-locking phenomenon is assumed to be the neural foundation of the limited capacity of short-term memory (Axmacher et al., 2010; Freunberger et al., 2011; Lisman, 2005; Lisman & Idiart, 1995). Furthermore, applying transcranial alternating current stimulation (tACS) over the sensorimotor cortex to induce pronounced gamma activities at the peak of theta oscillations can substantially enhance motor skill acquisition (Akkad et al., 2021). These findings suggest that the manner in which low-frequency oscillations modulate high-frequency activities in PAC effect reflects the neural signatures of brain regions underlying specific cognitive processes.

In rodents and humans, hippocampal place cells and entorhinal grid cells exhibit a theta phase precession effect, characterized as cells firing at progressively earlier phases of the local theta oscillations when a subject is going through the place field of a corresponding cell (Hafting et al., 2008; Qasim et al., 2021; Skaggs et al., 1996). Theta phase-precession effect relative to the hippocampal theta rhythm has also been reported in the ventral striatum and lateral septum (Lansink et al., 2016; Tingley & Buzsáki, 2018; van der Meer & Redish, 2011). Interestingly, the phase-precession effect in the ventral striatum is selectively associated with increased anticipatory activity towards reward sites, suggesting that it may strengthen the link between spatial information and reward representations (Lansink et al., 2016; Speers et al., 2022; Tingley & Buzsáki, 2018; van der Meer & Redish, 2011). In humans, the phase precession effect relative to a specific goal has also been unveiled for non-spatially tuned neurons in the frontal cortex, which also hints the role of phase precession effect in predicting forthcoming events (Qasim et al., 2021). So far, the studies of phase precession effect are mainly at the microscopic level of brain signal (i.e., single unit activities). How this effect manifest at the macroscopic level of brain signals and its relevance to reward expectancy remains unclear. In the present study, we recorded iEEG data from presurgical epilepsy patients when they were navigating a virtual T-maze with pre-defined rewards. Utilizing PAC analysis and representational similarity analysis (RSA), we investigated the neural dynamic in the AIC during the period proximal to the appearance of rewards to reveal the electrophysiological mechanisms underlying reward expectancy.

Results

To investigate the electrophysiological mechanisms of reward expectancy in the AIC, we tested eight epilepsy patients with 24 AIC contacts of implanted electrodes (18 in the right hemisphere; Figure 1A; Table S1). As a control, we also examined 19 hippocampal contacts, 7 contacts from 3 patients with AIC contacts and 12 contacts from 4 new patients. Subjects were asked to navigate a virtual T-maze and collect rewards while we recorded iEEG activities (Figure 1B-D). Subsequently, we examined iEEG activities time-locked to entering the reward zone (ERZ event) when the reward appeared on the monitor (Figure 1D). We also analyzed iEEG data time-locked to picking up the reward (PR event) and entering the decision zone (EDZ event) as control analyses. The number of included trials for different conditions were matched (31.92±2.43 [mean±SD] for ERZ, 32.08±2.47 for PR, and 32.17±2.48 for EDZ; $F_{(2, 33)} = 0.046$, $p = 0.95$; one-way ANOVA; Figure 1E; see *Methods - SEEG Data Acquisition and Preprocessing*). For each trial, subjects' response time (RT) to the rewards were calculated for further analyses (Figure 1F; see *Results - Functional relevance of PPLEs*).

Prevalence of Theta Oscillations in the AIC

Before performing further analyses on the oscillatory data, we first evaluated the presence of meaningful slow oscillations in the AIC. To do this, we identified low-frequency oscillations (LFOs) using the Multiple Oscillation Detection Algorithm (MODAL; see *Methods - Oscillation Detection*) (Watrous et al., 2018) and observed relatively constant and pronounced LFOs for time windows centered around the ERZ event (Figure 2A-C). The most prevalent LFOs fell in theta band (3.5Hz to 7.5Hz), which were detected in 41.70±1.07% (mean±SD) of time bins on average across subjects (Figure 2D, E; Figure S1). We also found LFOs in alpha (10Hz to 11Hz; 6.95±1.00%) and beta (13.5 Hz to 14 Hz; 4.67±0.51%) bands, which were less prevalent than LFOs from the theta band (Friedman test: $p = 3.35\times10^{-4}$; Wilcoxon matched-pairs signed rank test: $ps \leq 0.009$). As for the trial-level prevalence, LFOs in theta band were detected in almost all trials (99.58±1.18%, [mean±SD]), which was significantly higher than the prevalence of the other LFOs (alpha band: 45.41±6.27%; beta band: 51.34± 6.21%, Friedman test: $p = 1.53\times10^{-3}$; Wilcoxon matched-pairs signed rank test: $ps < 0.008$; Figure 2F, G). Similar results were found in time windows locked to PR and EDZ events in the AIC, as well as all events in the hippocampus (Figure S1). The prevalence of theta oscillations is consistent with previous findings showing theta activities in various brain regions during virtual navigation (Bohbot et al., 2017; Kahana et al., 1999; Watrous et al., 2018) and spontaneous theta oscillations in the insula during resting state (Das et al., 2022).

Coupling between Theta Phases and Gamma Amplitudes in the AIC when Approaching Rewards

To estimate the neural dynamics of the AIC during reward expectancy, we compared the PAC effect before and after entering the reward zone (pre- and post-ERZ events). The time course of phases for each low frequency ($frequency_{low}$;1-15Hz with 1 Hz as a step) and the time course of amplitudes for each high frequency ($frequency_{high}$; 30-150Hz with 5 Hz as a step) were extracted separately for time windows of pre- and post-ERZ events for each trial. The PAC strength was subsequently calculated between each low-frequency and each high-frequency for pre- and post-ERZ events within each trial. Using a multilevel linear regression analysis by considering the variance at contact and subject levels, we computed the difference of the PAC values between pre- and post-ERZ events for each $frequency_{low}$-$frequency_{high}$ pair. To correct errors caused by multiple comparisons, we used a cluster-based permutation analysis to extract $frequency_{low}$-$frequency_{high}$ clusters showing significant coupling when subjects were approaching the rewards (Zhang, 2023) (see *Methods - Phase Amplitude Coupling Analysis*). We found that the coupling between theta phases (5-7 Hz) and gamma amplitudes (80-105 Hz) was stronger during pre-ERZ events compared to post-ERZ events ($p_{corrected} = 0.047$, Figure 3A). We applied the same analysis to control conditions (i.e., pre-PR and pre-EDZ events) in AIC contacts and to all conditions in hippocampal contacts but did not find any meaningful clusters. Specifically, two significant PAC clusters were observed in pre-PR period in the hippocampus (Figure S2A). However, the low frequencies of these clusters were outside the oscillations detected using MODAL and therefore these clusters were considered meaningless (Watrous et al., 2018). We also applied an ROI approach to assess the mean PAC strength within the cluster shown in Figure 3A before and after each event for PR and EDZ conditions in the AIC and all conditions in the hippocampus. No differences of the PAC strength were found between before and after each event ($ts < 2.38$, $ps > 0.055$, Figure S2B). These results suggest that PAC effect occurs when approaching rewards, specifically in the AIC.

It is plausible that the observed enhanced coupling between theta phases and gamma amplitudes within the AIC during pre-ERZ periods contributes to reward expectancy. However, the enhanced PAC effect is possibly caused by the reduced PAC strength of post-ERZ period. To rule out such a possibility, we simulated a PAC distribution as baseline by performing a permutation analysis and compared the PAC strength of pre- and post-ERZ events with the simulated baseline PAC strength. Within each permutation, we shuffled the trials labels of time courses for high frequencies within each contact and computed the PAC values based on shuffled data. We then extracted the mean PAC value within the $frequency_{low}$-$frequency_{high}$ cluster reported in Figure 3A. The permutation procedure was repeated 500 times, generating 500 permuted PAC values. The baseline PAC was averaged across all 500 permuted PAC values within each trial. We also computed the empirical mean PAC strength within the $frequency_{low}$-$frequency_{high}$ cluster reported above for each pre- and post-ERZ event.

Subsequently, we compared the empirical PAC strength of pre- and post-ERZ events with simulated baseline PAC strength by performing paired t-tests across subjects (Figure 3B). The result showed that the PAC strength of pre-ERZ events was significantly greater than the baseline PAC ($t_{(7)} = 2.46$, $p = 0.043$), whereas the PAC strength of post-ERZ events was smaller than the baseline ($t_{(7)} = 2.70$, $p = 0.031$). As expected, the PAC of pre-ERZ events was higher than post-ERZ events in the AIC ($t_{(7)} = 3.71$, $p = 0.0075$). These results suggest that PAC effect in the AIC was caused by the enhanced PAC strength during pre-ERZ periods.

Additionally, we performed a control analysis by concatenating pre-ERZ periods from all trials within each subject and computed the PAC strength from the concatenated data. It is striking that no significant PAC cluster was found ($ps_{corrected} > 0.89$). It suggests that the underlying characteristics of PAC effect varies over trials, causing the PAC effect to disappear in the concatenated data. The variability of PAC effects over trials might arise from two sources. First, distinct gamma frequency bands may exhibit coupling with the same theta phases across different trials. Second, the maximal phase, corresponding to peak gamma power, varied across trials. We tested the first possibility by examining the distribution of the gamma frequencies with peak gamma power over trials for each contact. All 24 contacts showed a significant concentration of the peak gamma frequency at 80 Hz (Figure S3A), accounting for 77.60±1.44% (mean±SEM) of the total distribution which exceeded the probability density of a uniform distribution (i.e., 16.67%; $p < 0.001$, Wilcoxon signed rank test; Figure 3C). It suggests that the disappearance of PAC effect in concatenated data was not due to the dispersed distribution of peak gamma activities over trials, which ruled out the first possibility. The second possibility was tested by examining the distribution of the maximal theta phase in the trial-dependent PAC effect. We found that the maximal theta phases were evenly distributed in all AIC channels ($ps \geq 0.06$, Rayleigh test; Figure 3D, S3B). It suggests that the maximal theta phases of PAC effect vary across trials.

Taken together, these results suggested that gamma band activities coupled to theta oscillations during pre-ERZ period within each trial, specifically for contacts located in the AIC. Moreover, it also implies that the coupled theta phases vary across trials, which will be further examined in the subsequent section.

Gamma Activities Exhibit Phase-precession-like Effects in the AIC when Approaching Rewards

The result reported above suggests that gamma activities are coupled to different phases of theta oscillations across trials when subjects are approaching the same rewards. Hereby we looked further into the characteristic of PAC data to examine the dynamics of the maximal theta phases across trials. We therefore aimed to investigate if gamma activities were coupled to theta phases that systematically shifted forward when subjects were approaching a reward. To this end, we performed a circular-linear regression analysis between maximal theta phases of PAC effects during the pre-ERZ periods and the number of trials in individual AIC contacts (See *Methods - Phase-Precession-Like Effect of Gamma Activities*) (Qasim et al., 2021). If the peak gamma

power is coupled to gradually shifted theta phases when approaching rewards, we would expect a positive or negative correlation between the maximal theta phase (circular data) and the trial number (linear data). Indeed, we observed a significant negative correlation in 14 out of 24 (58.33%) AIC contacts from 7 out of 8 (87.5%) subjects and no correlations in the other 10 contacts (Figure 3E-G). The prevalence of such a negative correlation at either contact or subject level was significantly higher than chance level (i.e., 5%; both *ps* $<10^{-8}$, Binomial test) (Qasim et al., 2021). It suggests that peak gamma power couples to gradually earlier theta phases when approaching the same reward. The phenomenon is reminiscent of the phase prerecession effect and was termed as phase-precession-like effect (PPLE). To distinguish it from the other PPLE mentioned below, this PPLE was termed as $PPLE_{PAC}$. It is possible that $PPLE_{PAC}$ was caused by peak gamma power locked to systematically later time periods across trials. To test this possiblity, we computed the time of peak gamma power of each trial and tested if it was systematically shifted across trials. The result showed no significant correlation between time points of peak gamma power and the number of trials in any AIC contacts (all *ps* ≥ 0.065). It suggests that the $PPLE_{PAC}$ is an internal neural activity when approaching rewards, rather than simply driven by estimating the timing of the onset of rewards.

The $PPLE_{PAC}$ in the AIC when approaching rewards was possibly the electrophysiological foundation of reward expectancy. Meanwhile, it might also relate to the expectancy of visual stimuli, specific locations, or outcomes of picking up rewards. To determine whether $PPLE_{PAC}$ in the AIC was specifically related to reward expectancy, we compared the prevalence of $PPLE_{PAC}$ during pre-ERZ events with two control conditions (i.e., pre-PR or pre-EDZ events; Figure 3G). The results showed that the presence of $PPLE_{PAC}$ was observed in fewer AIC contacts during pre-PR (16.67% = 4/24, $p = 5\times10^{-6}$, Binomial test) and pre-EDZ (25% = 6/24, $p = 5\times10^{-4}$) events in comparison to pre-ERZ events. At the subject levels, a similar pattern was observed, demonstrating a lower occurrence of $PPLE_{PAC}$ during pre-PR events (25% = 2/8, $p = 4\times10^{-4}$) and a slightly lower occurrence during pre-EDZ events (50% = 4/8, $p = 0.07$) in comparison to pre-ERZ events. These findings suggest that the $PPLE_{PAC}$ in the AIC is preferred to reward expectancy rather than reward outcomes (i.e., pre-PR events) or non-reward visual stimuli or specific locations (i.e., pre-EDZ events).

To determine if $PPLE_{PAC}$ prior to reward appearance is specific to the AIC, we examined the prevalence of $PPLE_{PAC}$ in contacts located in the hippocampus during the pre-ERZ event (Figure 3F, G). The results showed that fewer contacts exhibited $PPLE_{PAC}$ in the hippocampus (6/19, 31.58%) compared to that in the AIC ($p = 0.0061$, Binomial test). Additionally, numerically smaller number of subjects showed $PPLE_{PAC}$ in hippocampal contacts (4/7, 57.14%) than the number of subjects showed $PPLE_{PAC}$ in AIC contacts ($p = 0.079$). It suggests that $PPLE_{PAC}$ during pre-ERZ periods is more preverlent in the AIC than in the hippocampus.

In addition, we computed the presence of $PPLE_{PAC}$ in AIC subregions (see *Methods - Electrode Reconstruction*) and found that the prevalence of $PPLE_{PAC}$ was highest in the dorsal AIC (Figure S4A, C; see *Supplementary information*). All together, the $PPLE_{PAC}$ reveals that gamma activities peak at progressively earlier theta phases

when subjects approaching rewards. Futhermore, such a reward-expectancy-related $PPLE_{PAC}$ is especially prominent in the AIC.

Pre-activation of the Reward-specific Brain Patterns Exhibits PPLE in the AIC when Approaching Rewards

An expectancy of receiving rewards indicates that the brain starts to process reward-relevant information before the onset of rewards. Thus, we hypothesized that the brain patterns representing rewards would be activated prior to the onset of actual rewards. To test this hypothesise, we investigated the pre-activation of reward-specific representations in AIC contacts before reward onset using representational similarity analysis (RSA) (Kriegeskorte et al., 2008; Xue et al., 2010; Zhang et al., 2018). We first computed the reward-specific representations by calculating the neural similarities between the post-ERZ periods at different locations (the central and two lateral roads; $RSA_{ERZ/ERZ}$; Figure 1B right panel). We also calculated the neural similarities between the post-ERZ and post-EDZ period ($RSA_{ERZ/EDZ}$; Figure 4A; see *Methods - Computing Reward-Specific Brain Patterns*) as baseline. The reward-specific neural patterns were subsequently identified from the post-ERZ period by comparing the differences between $RSA_{ERZ/ERZ}$ values and the average $RSA_{ERZ/EDZ}$ value (Figure 4B). We observed that neural activities within the time window from 1.04 to 1.16 second following the onset of a reward were more similar between pairs of post-ERZ events than between post-ERZ and post-EDZ events ($p_{corrected} < 0.001$). It indicates the presence of reward-specific effects.

To examine the pre-activation of reward-specific brain patterns, we computed the neural similarities between each time window of the pre-ERZ events at the central road and reward-specific brain patterns during post-ERZ periods at lateral roads. To avoid the temporal proximity effect (i.e., autocorrelations), correlations between pre- and post-ERZ periods from the same trial were excluded. The Fisher-z transformed correlation values were averaged across pre-ERZ time windows and trials. For all contacts, the averaged similarities between neural patterns of pre-ERZ period and the reward-specific brain pattern was significantly greater than zero ($t_{(23)} = 8.27$, $p < 0.001$; Figure 4C). This suggests that the reward-specific brain pattern was pre-activated before the onset of rewards.

Subsequently, we examined if the pre-activation of reward-specific neural patterns also showed PPLEs (Qasim et al., 2021). Theta phases of individual trials were extracted from the highest pre-activation time windows (Figure 4D; see *Methods - PPLE of the Pre-activation of Reward-Specific Patterns*). We conducted a circular-linear correlation between trial numbers and the extracted theta phases over trials within each contact (Figure 4E). PPLEs were observed in 29.17% (7/24) of AIC contacts from 50% (4/8) of subjects for the pre-activation of the reward-specific pattern, all of which exceeded the chance level (*ps* < 0.006, Binomial test; Figure 4F). This suggests that the pre-activation of reward-specific brain patterns was coupled to earlier theta phases over trials, showing PPLEs. We termed as $PPLE_{RSA}$ in order to distinguish it from $PPLE_{PAC}$.

PAC effects were related to pre-activation of the Reward-specific Brain Patterns

As reported above, both PAC effects and pre-activation of reward-specific brain patterns exhibited PPLEs when approaching rewards. Naturally, we investigated the relations between PAC effects and pre-activation of reward-specific brain patterns. The peak gamma power of PAC effect occurred at 1.02±0.09 second (mean ±SEM) before the onset of rewards, which was not differ from the time when the highest pre-activation took place (1.04±0.12 second before the onset of rewards; $t_{(23)} = 0.72$, $p = 0.48$; Figure 4G). It indicates that the pre-activation of reward-specific representations and the peak gamma power tend to occur at similar time. Furthermore, we conducted a comparison of gamma power between the timepoints exhibiting the highest and lowest pre-activation levels of the reward-specific representation within each trial. Significantly higher gamma power was observed in relation to the peak pre-activation of reward-specific patterns compared to the trough pre-activation of these patterns ($p < 0.001$, Wilcoxon matched-pairs signed rank test; Figure 4H). We also performed a similar analysis to compare theta phases corresponding to the peak pre-activation of reward-specific representations and maximal theta phases of PAC effect, and found no differences between them ($p = 0.62$, Rayleigh test). These findings provide supporting evidence that the pre-activation of reward-specific representations occurs approximately same time with PAC effect.

Additionally, we also checked the relation of the strength between two PPLEs and found that $PPLE_{RSA}$ were numerically positively related to $PPLE_{PAC}$ over subjects ($r = 0.59$, $p = 0.14$; Spearman's correlation; Figure 4I). In detail, 4 out of 8 subjects were found exhibiting both $PPLE_{RSA}$ and $PPLE_{PAC}$. Subjects #4, #12 and #17 showed only $PPLE_{PAC}$, while subject #7 did not exhibit either PPLE. Moreover, $PPLE_{PAC}$ and $PPLE_{RSA}$ exhibited a comparable spatial distribution within the AIC (Figure S4; see *Supplementary information*). Taken together, these findings indicate that the pre-activation of reward-specific representations occurs concurrently in time and space with PAC effects.

Functional Relevance of PPLEs

The high prevalence of PPLEs in the AIC preceding ERZ events suggests a potential role for PPLEs in reward expectancy. Previous studies have shown that reward anticipation facilitates cognitive performance, such as shortening the response latency (Baruni et al., 2015; Hermoso-Mendizabal et al., 2020). We thus investigated if PPLEs facilitated subjects' responses to rewards. In order to examine the improvement of RT across trials, z-transformed RT was extracted for each trial in each subject (Figure 5A and S5). Trials with a z-score > 3 were excluded from further data analysis. We then performed a linear regression analysis to predict the z-transformed RT of picking up rewards using the number of trials. RTs trended down for all eight subjects with

AIC contacts as the number of trials increased ($\beta s < 0$; Table S2 and Figure 5B, S5). We tested the significance of the RT decline pattern by performing a surrogate analysis on each subject. Within each permutation, we randomly shuffled the trial numbers, computed the linear regression again, and obtained a surrogate coefficient. The permutation procedure was repeated 500 times, generating 500 surrogate coefficients. We then ranked the empirical coefficient within the distribution of the surrogate coefficients for each subject. We observed a significant decrease in RT with increasing number of trials in five subjects ($ps < 0.05$; Figure S5). All of these subjects exhibited $PPLE_{PAC}$, while three additionally manifested $PPLE_{RSA}$. In the other two subjects exhibiting PPLEs, the z-transformed RT and the number of trials were numerically negatively related to each other (subject #16: $\beta = -0.21$, $p = 0.13$; subject #17: $\beta = -0.04$, $p = 0.40$). As for subject #7, who did not show any PPLEs, RT showed a subtle decline as the number of trials increased ($\beta = -0.01$, $p = 0.46$). The results imply that the shortened response latency is related to PPLEs in the AIC.

To find evidence supporting the association between PPLEs and behavioral performance, we computed the correlation coefficient between the strength of PPLEs and the magnitude of performance improvement. PPLE strength for each subject was determined by calculating the average absolute value of the circular-linear coefficients across AIC contacts for either $PPLE_{PAC}$ or $PPLE_{RSA}$. The parameter representing behavioral improvement was identified as the magnitude of unstandardized coefficients (i.e., the slope for the fitted lines) obtained from the linear regression analysis in which we forecasted z-transformed RTs with trial numbers (Figure 5A, S5 and Table S2). We performed the Spearman's correlation between $PPLE_{PAC}$ strength and the behavioral improvement over subjects and found a significant positive correlation ($r = 0.78$, $p = 0.03$; Figure 5B). It suggests that a stronger $PPLE_{PAC}$ relates to a greater improvement in subjects' performance. We performed a corresponding analysis to $PPLE_{RSA}$ and found a numerically positive correlation between the behavioral improvement and $PPLE_{RSA}$ strength ($r = 0.50$, $p = 0.22$). Additionally, RT variability is an index of performance reliability, with a smaller value indicating more consistent RTs and fewer random errors, thus reflecting better behavioral performance (Epstein et al., 2011). We calculated coefficients of variations (CV) for each subject and compared the difference of CVs between subjects with and without PPLEs in the AIC. The result showed that the subjects exhibiting $PPLE_{PAC}$ presented more stable performance with significantly smaller CVs than the subject without $PPLE_{PAC}$ (26.43±6.54% [mean±SD] vs. 56.93%; $t_{(6)} = -12.35$, $p = 0.001$; one-sample t-test followed by Bootstrap sampling; Figure 5C). Meanwhile, a numerically smaller CV was found in subjects with $PPLE_{RSA}$ comparing subjects without $PPLE_{RSA}$ (25.90±5.20% vs. 34.58±16.72%, $t_{(6)} = 0.99$, $p = 0.37$; independent sample t-test followed by Bootstrap sampling).

Collectively, PPLEs, especially $PPLE_{PCA}$, exhibit a strong correlation with enhanced behavioral performance characterized by improved response stability and higher reaction speed.

Discussion

Reward expectancy facilitates various cognitive processes, such as attention, memory, and motivation (Baruni et al., 2015; Frömer et al., 2021; Rowe et al., 2008). To explore the neural basis of reward expectancy, we investigated iEEG activities in the AIC when approaching the destined reward in a virtual T-maze. Firstly, we reported that gamma activities were coupled to different theta phases over trials in the AIC when approaching rewards. Meanwhile, the reward-specific representations in the AIC were pre-activated prior to the appearance of the reward. Such pre-activation tended to occur approximately the same time as the peak gamma activities in individual trials. Interestingly, both the peak gamma activities and the highest pre-activation of reward-specific brain patterns were locked to earlier theta phases across repetitions of approaching the same reward, exhibiting PPLEs. Furthermore, PPLEs is functionally relevant, showing that the strength of PPLEs is related to the magnitude of the behavioral improvement. The identification of PPLEs within the AIC provides valuable insights to better understand the electrophysiological mechanism underlying reward expectancy.

The Functional Role of AIC in Reward Expectancy

Recent neuroimaging evidence has revealed the involvement of AIC at an early stage of reward processing (Apaydın et al., 2018; O'Doherty et al., 2002; Schneider et al., 2018). Additionally, invasive studies of non-human primates have reported a class of responsive neurons in the AIC that fire in anticipation of an immediate reward (Mizuhiki et al., 2012). It was reported in the present study that reward-specific neural patterns in the AIC were preactivated before subjects entering the same reward zone, which provides compelling evidence supporting the functional role of the AIC in reward expectancy (Kok et al., 2014).

The AIC, similar to other brain regions involved in reward processing, contains a high concentration of dopamine which aids in predicting when and how rewards will occur (Allman et al., 2005; Hurd et al., 2001), thereby contributing to our anticipation of future rewards. Of note, the role that the AIC plays in reward processing is distinctive. In contrast to other reward-related brain regions such as the anterior cingulate cortex and ventral striatum, the AIC exhibits expectancy-related activities that are unaffected by the validity of the expected reward (Mizuhiki et al., 2012). A plausible explanation is that the role of the AIC in reward expectancy extends to a broader spectrum of cognitive processes beyond mere reward prediction (Schneider et al., 2018). The AIC is widely recognized for its significant involvement in various cognitive processes, including information integration, salience identification, and attention allocation (Kurth et al., 2010; Mesulam & Mufson, 1982; Molnar-Szakacs & Uddin, 2022; Sun et al., 2020). In particular, due to its extensive connections with diverse limbic and neocortical regions, the AIC integrate bottom-up contextual information with top-down prior knowledge, such as representations of context-reward associations. Consequently, the AIC plays a vital role in developing comprehensive understandings of contexts and shaping expectations

regarding rewards (Bein et al., 2023; Molnar-Szakacs & Uddin, 2022; Uddin et al., 2014). This integration process can be referred to as the establishment and reinforcement of context-reward association (Sun et al., 2020), resulting in an enhanced salience of expected rewards and a heightened allocation of cognitive resources (e.g., attention and motivation) towards those rewards (Frömer et al., 2021; Schneider et al., 2018). In the current study, we observed a robust PAC between theta phases and gamma amplitudes in the AIC prior to the presentation of the actual reward, which may reflect the underlying mechanisms of information integration during reward expectancy (Mariscal, Berry-Kravis, et al., 2021). Furthermore, the peak gamma activities, where PAC was established, tended to occur approximately the same time as the pre-activation of reward-specific brain patterns. It suggests that the integration between the current input of the context information and prior knowledge of context-reward associations is intimately related to the activation of neural patterns representing rewards, which in turn enhances the context-reward association (Kok et al., 2014; Sun et al., 2020). These findings strengthen the evidence for the functional engagement of the AIC in anticipating forthcoming rewards, which is achieved through the establishment of context-reward association and the allocation of cognitive resources based on salience (Frömer et al., 2021; Sun et al., 2020). Our study provides the first evidence of electrophysiological mechanisms of the AIC in reward expectancy in humans. However, the causal relations of the sub-processes of reward expectancy remains un-addressed in the current study, which needs to be studied in further research.

Phase Precession Effect of Macroscopic Brain Signals

The phase precession effect is first reported in brain signals at microscopic levels. Specifically, single units are activated in gradually earlier phases over successive theta cycles of sustained local field potentials (Jones & Wilson, 2005; O'Keefe & Recce, 1993). It is considered to be crucial for compressing slower behavioral sequences to faster neural activity (Jones & Wilson, 2005; O'Keefe & Recce, 1993; Reifenstein et al., 2021) and predicting the forthcoming stimuli (Qasim et al., 2021; van der Meer & Redish, 2011).

High gamma activities refer to rapid neural oscillations and is an effective proxy measure of single neuron activities at the macroscopic level (Belitski et al., 2008; Ray & Maunsell, 2011). Nevertheless, there is limited evidence for the theta phase precession effect of high gamma activities. Recently, Zheng and colleagues have investigated the cross-regional theta-gamma interactions during facial perception using the contextual modulation task and reported a macroscopic-level effect analogous to theta phase precession (Zheng et al., 2022). This observation not only expands the phenomenon of theta phase precession from a microscopic level (i.e., spikes of single units) to a macroscopic level (i.e., high gamma activities of neuronal ensembles), but it also further broadens the neural representation of non-spatial states (e.g., task stages from context maintenance to face perception). Inspiringly, our results also unveiled a particular temporal structure of neural activities in the AIC at a macroscopic level during reward expectancy. Specifically, both the peak gamma activities and

the highest pre-activation of reward-specific patterns were found to be locked to earlier theta phases when approaching rewards across trials. Such forward shift of theta phases is reminiscent of theta phase precession effect and termed PPLEs (Akkad et al., 2021; Kragel et al., 2020; Lopes-Dos-Santos et al., 2018; Qasim et al., 2021; Reddy et al., 2021; Yang et al., 2021). Our findings of PPLEs hold important implications for exploring theta phase precession effects of neural activities at multiple spatial (i.e., from single-unit recordings to high gamma activities and brain patterns) and temporal (i.e., from milliseconds to minutes) scales.

More exactly, PPLEs in the AIC were related to reward expectancy, rather than reward outcome or any particular stimulus or location, which further supports the involvement of the AIC in reward expectancy. In contrast, PPLEs in the hippocampus did not exhibit any preference for reward expectancy. This finding is analogous to the observation in rodents that hippocampal phase precession is uniformly distributed and not affected by reward expectancy (Lansink et al., 2016; van der Meer & Redish, 2011). Nevertheless, the exact relationship between the PPLEs and phase precession effect remains unclear, due to lacking simultaneous recordings at micro- and macroscopic levels. Future studies combining macro- and micro-electrodes are valuable to determine whether the PPLEs have the same spatiotemporal distribution and functional role as theta-phase precession.

Reward Expectancy Promote Behavioral Performance

Reward expectancy has been suggested to significantly contribute to allocating cognitive resources (Baruni et al., 2015; Frömer et al., 2021; Lansink et al., 2016), resulting in quicker and more accurate responses to rewards in individual subjects (Rowe et al., 2008). A prerequisite for the facilitation effect of reward expectancy is to establish the context-reward association (Rowe et al., 2008). When subjects are placed in a particular context, neural representations of the context will be activated. It will in turn trigger the activation of neural representations of events associated with the context, such as a reward, which will further induce reward expectancy (Bein et al., 2023). The expected reward occupies a large amount of attentional and motivational resources for its salience from contextual information and aids in the preparation of reactions to forthcoming rewards (Bein et al., 2023; Frömer et al., 2021; Schneider et al., 2018). As a result, subjects are more likely to exhibit improved performance due to the preceding preparation of the motor response, characterized by quicker response and higher accuracy levels (Kok et al., 2014). Additionally, the reward appearance consistent with expectation would in turn enhance the established context-reward association (Rowe et al., 2008; Sun et al., 2020). In the present study, the pronounced theta phase-gamma amplitude coupling and pre-activations of reward-specific patterns might imply the establishment of a context-reward association when approaching rewards. Therefore, we assumed that the presence and strength of PPLEs reflected the level of reward expectancy. We then made a preliminary exploration of the behavioral significance for PPLEs in the AIC. Results from our study indicated that PPLEs bear a potentially positive

influence on behavioral performance (e.g., quicker and more stable response speed), highlighting the important role of reward expectancy in improving behavioral outcomes (Frömer et al., 2021; Pessiglione et al., 2007; Rowe et al., 2008). Our discovery sheds lights on the potential implementation of neuromodulation techniques to enhance PPLEs and thus promote cognitive capabilities.

In future research, there exists a remarkable opportunity to craft meticulously refined experimental tasks that encompass a diverse array of rewards. These rewards may comprise not only psychological and material incentives but also encompass variations in their intensity and efficacy. By embracing such rich and multifaceted experimental designs, we can pave the way for a more precise identification of the optimal spatiotemporal characteristics underpinning neural activity associated with reward expectancy. Consequently, this heightened understanding will empower us to precisely modulate reward expectancy effect and ultimately enhance behavioral performance.

Conclusions

In summary, we reported that PAC effects between theta phase and gamma amplitude tend to occur simultaneously with the pre-activation of reward-specific patterns during the expectation period of a forthcoming reward, suggesting that AIC plays a crucial role in reward expectancy. Further, we identified the neural pattern of PPLEs, showing that both the peak gamma activities and highest pre-activation of reward-specific patterns progressively coupled to an earlier phase of the theta oscillations as the number of trials increased. More importantly, this neural mechanism promotes behavioral performance. PPLEs were considered the unique potential mechanism for AIC in modulating reward expectancy.

Methods

Subject Details

Twelve medically refractory epilepsy patients with depth electrodes for diagnosis (half males; average age = 25.25±8.87 years [mean±SD]; Table S1) were recruited from the Hôpital de la Salpêtrière in Paris and the Second Affiliated Hospital of Zhejiang University in China. The study was approved by the Medical Ethics Committee at the hospital sites (INSERMC11-16 and StudyNo.2020-910, respectively), and written informed consent was obtained from all subjects.

Experimental Design

We built a virtual T-maze (Panda3d and PandaEPL) in which subjects could freely navigate. As illustrated in Figure 1B, the T-maze consisted of 2 lateral roads, a central road, a starting zone, a decision zone, and three reward zones. The starting zone was both the beginning and the end of each trial. At the decision zone, subjects chose the correct direction to the lateral road according to the sign on the wall (circle or triangle represents left-turn or right-turn, respectively, Figure 1C, D). Among three reward zones, one was on the central road where a gold coin (value of 0.15 Euros) would definitely appear, and two were on the lateral roads where a gold coin appeared only if subjects chose the correct direction at the decision zone. Once the gold coin appeared, subjects were encouraged to press the Enter button to pick it up. Otherwise, the reward disappeared after subjects navigated through the reward zone. Subjects were encouraged to collect enough gold coins (10 Euros) as soon as possible. To avoid being disoriented, subjects were asked to memorize as many pictures hanging on the wall as possible to encourage them to pay attention to the task and their on-going position. Furthermore, different paintings of wallpapers also helped subjects to allocate themselves inside the maze to avoid being disoriented (as indicated in Figure 1D). We tested their knowledge about the location of pictures at the end of the experiment (data not reported here).

During the experiment, subjects were sitting in their beds with a laptop on a table in front of them. They used arrow buttons on the keyboard to navigate the virtual maze (Figure 1C). The full linear running speed was 6 virtual units/second and the linear acceleration speed was 40 virtual units/second^2. The distance from the center of the starting zone to the center of the decision zone was 32 virtual units (Figure 1B). The distance from the center of the left arm to the center of the right arm was 24 virtual units. The width of the corridor was 4 virtual units. Every time subjects picked up the reward or entered the decision zone, they paused for 2 seconds before continuing navigating. The left- and right-turn signs at the decision zone were counter-balanced within each subject. During the experiment, the testing laptop sent triggers to iEEG recording system in order to synchronize behavioral and iEEG data offline.

Experimental Procedure

At the beginning of each trial, subjects were standing at the starting location (Figure 1D). They first navigated through the middle arm of the T-maze toward the decision zone. On the middle arm, they encountered the first reward. Subsequently, subjects proceeded to enter the decision zone located at the other end of the middle corridor. Immediately after entering the decision zone, a triangle or a circle was signed on the wall. Subjects were asked to turn to the correct lateral arm in order to pick up the second reward of that trial. If they made a wrong choice at the decision zone (i.e., running into a wrong arm), the second reward of that trial would not appear. At the end of each trial, they navigated back to the starting zone for the next trial. Before the experiment,

subjects performed a practice session by going through a different maze to familiarize themselves with the procedure of the experiment and navigating in the virtual environment.

Behavioral Data Collection and Process

During the experiment, navigation trajectories of subjects were logged. We focused on three events as three experimental conditions for further behavioral and iEEG data analysis: entering the reward zone (ERZ), picking up the reward (PR) and entering the decision zone (EDZ). When subjects entered the reward zone (ERZ), a gold coin would appear on the monitor. The event corresponding to PR was defined as the moment when subjects pressed the Enter button to collect rewards. Additionally, upon EDZ, a picture would be displayed on the wall. To minimize the influence of learning biases, we specifically focused on the reward zone in the central corridor, where subjects' expectations for receiving a reward were consistently fulfilled (i.e., the reward would certainly appear). Another advantage is ensuring a rough balance among the trial numbers under the three conditions included in the analysis. Nevertheless, the ERZ events occurred on the lateral roads were extracted to identify the reward-specific neural patterns (Figure 4A, see *Method - Computing Reward-Specific Brain Patterns*).

As a behavioral parameter, the response latency for picking up a reward was calculated for each ERZ event, referring to the time interval between the appearance of a gold coin and the button press to collect the coin in each trial (Figure 1F and S4).

Electrode Reconstruction

The AdTech electrodes used at the Hôpital de la Salpêtrière were equipped with 4-12 contacts, each measuring 1 mm in diameter, 2.41 mm in length, and spaced 5 mm apart (Lehongre et al., 2022). Meanwhile, the HKHS electrodes employed at the Second Affiliated Hospital of Zhejiang University consisted of 8-16 contacts, with a diameter of 0.8 mm, length of 2 mm, and an inter-contact distance of 1.5 mm (Chen et al., 2023).

Contacts located in the AIC and hippocampus, known to have close associations with reward processing and spatial memory (Kragel et al., 2020; Lopes-Dos-Santos et al., 2018; Rothkirch et al., 2014), were selected for further data analyses (Figure 1A). The AIC was defined as the part of the insular that precedes the central insular sulcus. It was divided further into four subregions according to the sulci: the anterior short gyrus (ASG), middle short gyrus (MSG), posterior short gyrus (PSG) and anterior inferior cortex (Faillenot et al., 2017) (Figure S4A). The three short gyri were collectively known as the dorsal AIC, while the anterior inferior cortex was considered the ventral AIC (Fathy et al., 2020). The exact location of each contact in AIC subregions was defined via visual inspection in the local space of each subject using FSLeyes (https://fsl.fmrib.ox.ac.uk/fsl/fslwiki/FSLeyes).

After removing contacts at seizure onset zones and those contaminated by epileptic spikes, we obtained 24 AIC contacts (18 in the right hemisphere) from 8 subjects and 19 hippocampal contacts (10 in the right hemisphere) from 7 subjects (Figure 1A and Table S1). Three subjects (subject #8, #14 and #15) had both AIC and hippocampal contacts.

IEEG Data Acquisition and Preprocessing

IEEG data was acquired using an Ad-Tech system (Hôpital de la Salpêtrière) and a Nihon-Kohden recording system (Second Affiliated Hospital of Zhejiang University) in a bipolar layout at sampling rates ≥1k Hz (Table 1). IEEG data were first down-sampled to 1kHz, bandpass filtered from 0.01 to 200 Hz, and notch filtered at 50 Hz and its harmonics. The filtered data were then re-referenced to the average activity of all depth electrodes outside seizure onset zones (Zhang et al., 2018). We segmented the iEEG data into epochs, spanning 2 seconds before to 2 seconds after each event of interest (i.e., ERZ, PR and EDZ). To remove any edge effects caused by time-frequency decomposition, one extra second before the start and after the end of each epoch was extracted. Data preprocessing was performed using EEGLAB toolbox (Delorme & Makeig, 2004) and custom MATLAB code.

Valid epochs were screened for each experimental condition. Epochs with breaks for clinical purposes (e.g., taking medicine; 1 epoch from subject #8 under the ERZ condition), missing rewards (i.e., running out of the reward zone without picking up the reward; 1 epoch from subject #15 under the PR condition), and incorrect responses at the decision zone (i.e., turning into a wrong arm; 4 epochs from subject #16 and 1 epoch from subject #17 under the EDZ condition) were excluded. Epochs contaminated by artifacts such as epileptic activities were detected by visual inspection and excluded from further data analysis. The numbers of trials included were 31.92±2.43 (mean±SD) for ERZ, 32.08±2.47 for PR, and 32.17±2.48 for EDZ, while the numbers of trials excluded were 4.25±2.83 for ERZ, 3.83±2.69 for PR, and 3.67±2.10 for EDZ.

Oscillation Detection

Using the Multiple Oscillation Detection Algorithm (MODAL) (Watrous et al., 2018), we explored the existence of low-frequency oscillations (LFOs) in each epoch for each contact, respectively (Figure 2, S1). Firstly, power spectral density (1–50 Hz in steps of 0.5 Hz) was calculated using Morlet wavelet transformation (6 cycles) for each trial within each contact. Then, a 1/f regression to the background spectrum was constructed in log-log space, and narrow-band oscillations exceeding the fitted line were identified (Watrous et al., 2018). To evaluate the prevalence of oscillations at each frequency, the percentage of detected time was calculated for each contact and each trial which were further averaged across contacts and trials for each experimental condition and subject (Figure S1).

Phase Amplitude Coupling (PAC) Analysis

In order to estimate the strength of PAC, we calculated the modulation index based on the mean vector length (mvlMI) (Canolty et al., 2006; Özkurt & Schnitzler, 2011; Seymour et al., 2017). To this end, we first filtered iEEG data using the finite impulse response (FIR) and obtained the dynamics of each low-frequency band (1-15 Hz in steps of 1 Hz; 15 samples; $\text{frequency}_{\text{low}}$) and each gamma band (30–150 Hz in steps of 5 Hz; 25 samples; $\text{frequency}_{\text{high}}$) for each ERZ trial (Delorme & Makeig, 2004). The instantaneous phases of the low frequency (ϕ) and the amplitudes of the high frequency (A) were extracted using the Hilbert transformation. We then computed the mvlMI metrics between the time course of the low-frequency phase and high-frequency power for time windows before and after each ERZ event separately using the formula as follows:

$$\text{mvlMI} = \frac{1}{\sqrt{tw}} \frac{\left|\frac{1}{tw}\sum_{t=1}^{tw} A(t) \times e^{i \times \phi(t)}\right|}{\sqrt{\frac{1}{tw}\sum_{t=1}^{tw} A(t)^2}}$$

in which t indicates each time point and tw indicates the total number of time points. This resulted in two mvlMI metrics (15 $\text{frequency}_{\text{low}}$ × 25 $\text{frequency}_{\text{high}}$) for each ERZ event, one for the pre-ERZ time window and the other for the post-ERZ window. To obtain a more robust and accurate estimate of PAC strength, the statistically normalized mvlMI values were calculated by performing a z-transformation of the empirical mvlMI values in the surrogate mvlMI distribution (Canolty et al., 2006; Özkurt & Schnitzler, 2011), separately for pre- and post-ERZ windows. The surrogate mvlMI data were generated by shuffling the amplitude time series within each trial.

Subsequently, we compared the normalized mvlMI values between pre- and post-ERZ periods using a multi-level linear regression analysis by considering the variance at both the subject and contact levels for each $\text{frequency}_{\text{low}}$-$\text{frequency}_{\text{high}}$ bin. Bins corresponding to a p level smaller than 0.05 were selected (Zhang et al., 2015). Adjacent bins were clustered together. The statistical value of each mvlMI cluster was the summed t value from the multi-level linear regression analysis. The significance level of the empirical mvlMI clusters was estimated using a cluster-based permutation analysis (Zhang, 2023). Within each permutation, we randomly shuffled condition labels (i.e., pre- or post-ERZ event) and performed the same multi-level linear regression analysis. This generated a set of surrogate mvlMI clusters. The mvlMI cluster with the largest statistical value was selected. The permutation procedure was repeated 500 times, generating 500 surrogate mvlMI clusters. The significant level of each empirical mvlMI cluster was estimated by ranking its statistical value within the distribution of 500 surrogate mvlMI clusters. If the statistical value of a cluster exceeded the 95th percentile of the surrogate mvlMI distribution, it was labeled as a significant cluster ($p < 0.05$). We applied the same analysis to the PR and EDZ conditions in contacts located at the AIC and hippocampus (Figure 3, S2).

Phase-Precession-Like Effect (PPLE) of Gamma Activities

To examine the trial-wise PAC, we computed PPLE by computing the dynamic of the low-frequency phases at which the high-frequency power peaked over trials. To this end, we first extracted the preferred low-frequency phases of the PAC analysis for the time window before each ERZ event. The ϕ_{PAC} was obtained using the following formula,

$$\phi_{PAC} = \text{angle}\left(\sum_{t=1}^{tw}(A(t)^2 \times \cos(\phi(t)) + A(t)^2 \times \sin(\phi(t)) \times i)\right)$$

in which *t* indicates each time point, *tw* indicates the total number of time points, *A* indicates the instantaneous amplitude of the high-frequency band, and ϕ indicates the instantaneous phase of the low-frequency band. This generated one ϕ_{PAC} for each ERZ event within each contact. We then conducted a circular-linear correlation within each contact (Qasim et al., 2021), in which the number of trials was taken as a linear parameter and the ϕ_{PAC} derived from the corresponding trial was taken as a circular parameter. The significance level of the coefficient value was estimated by performing a surrogate analysis. Within each permutation, we randomly shuffled trial labels and then computed the circular-linear correlation again (Zhang, 2023). This generated one surrogate coefficient value. The permutation was repeated 500 times and we obtained 500 surrogate coefficient values. If the circular-linear correlation coefficient derived from the empirical data exceeded the 95th percentile of the surrogate coefficient distribution, the empirical correlation value was considered significant, indicating the existence of PPLEs. We performed a control analysis by applying the same analysis to PR and EDZ events in AIC and hippocampal contacts.

Computing Reward-Specific Brain Patterns

To demonstrate that neural activities before appearance of rewards are relevant to reward expectancy, we tested if the reward representations were pre-activated before reward onset using representational similarity analysis (RSA) (Figure 4A) (Kriegeskorte et al., 2008; Xue et al., 2010; Zhang et al., 2018). We first identified reward-specific brain patterns by analyzing post-ERZ events at three different spatial locations, including the mid-arm, the left arm, and the right arm (Figure 1B). To do this, each post-ERZ event was segmented into 80ms windows with 40ms overlap. Thus, 49 windows were obtained for each post-ERZ period. For each time window, the iEEG power of low-frequency bands (1-30 Hz in steps of 1 Hz) and high-frequency bands (35–150 Hz in steps of 5 Hz) were concatenated (54 frequencies). It resulted in a 54 (frequency bins) × 49 (time bins) matrix for each post-ERZ event for each contact. Then, we computed the neural similarity between each post-ERZ/post-ERZ pair. To do this, brain patterns of each time window of one post-ERZ trial (*Trial m*) and every time window of another post-ERZ trial (*Trial n*) were compared by performing Spearman's correlations over frequencies in each contact. Fisher-z transformed correlation coefficients were averaged across all time windows of *Trial n*. We repeated the same procedure for all time windows of *trial m* and obtained a 1 × 49 (post-ERZ time bins) confusion matrix for each post-ERZ/post-ERZ pair and each contact ($RSA_{ERZ/ERZ}$). Note

that we excluded correlation coefficients between same trials and between trials at the same location in order to eliminate the temporal proximity effect and the confounding effect induced by representing the same location. We also extracted the brain pattern of the post-EDZ events and computed the neural similarities between each post-ERZ event (from three locations) and each post-EDZ event following the same procedure for each contact ($RSA_{ERZ/EDZ}$). Then, the $RSA_{ERZ/EDZ}$ values were averaged across all post-ERZ/post-EDZ pairs within each contact which was considered as baseline. We performed a multi-level linear regression analysis between $RSA_{ERZ/ERZ}$ values and the average $RSA_{ERZ/EDZ}$ value by considering the variance at both subject and contact levels for each post-ERZ time bin. A bin with $p < 0.05$ was selected. Selected bins were assigned to the same cluster if they were connected. The statistical value of each cluster was the summed t value from the multi-level linear regression analysis. Subsequently, the significance level of each cluster was estimated using cluster-based permutation analysis by randomly shuffling post-ERZ windows for 500 times (Zhang, 2023). For each permutation, we performed the same multi-level linear regression analysis and selected the cluster with the largest statistical value as the surrogate cluster. The significance level of the empirical clusters was estimated by ranking their statistical value within the distribution of 500 surrogate clusters. It was considered significant only if cluster size derived from the true data exceeded the 95th percentile of the surrogate distribution. The iEEG activities from time windows showing significant post-ERZ/post-ERZ similarities were regarded as the reward-specific brain patterns.

PPLE of the Pre-activation of Reward-Specific Patterns

If reward information was processed before reward onset, we assumed that the reward-specific brain patterns were pre-activated. In practice, we would expect to observe that the pre-ERZ brain patterns are similar to the reward-specific brain patterns, showing significant positive correlation coefficients. To compute the pre-activation of reward-specific brain patterns during pre-ERZ periods, we computed the neural similarity between brain patterns of each pre-ERZ time bin and the reward-specific brain pattern obtained above via Spearman's correlation for each contact and trial. This generated a time course of similarity values over pre-ERZ time windows. The Fisher-z transformed correlation coefficients were averaged over pre-ERZ time windows of each trial and contact. We then compared the correlation coefficients against zero using a multilevel linear regression analysis by considering the variance at contact and subject levels. If the correlation coefficient was larger than 0, it indicated that the neural pattern during pre-ERZ period was similar to reward-specific neural representations, which suggests pre-activation of reward-specific representations.

To further investigate the temporal structure of the pre-activation, we performed a similar PPLE analysis as in the above section. First, we identified the pre-ERZ time bin in which the neural pattern had the largest similarity to the reward-specific brain pattern for each trial and each contact. We then extracted the corresponding theta phases which resulted in one 1 × n (trial) phase matrix for each contact. Using previously

established algorithms (Qasim et al., 2021), we conducted a circular-linear correlation between the extracted theta phases and trial numbers within each contact. The significance level of the coefficient value was estimated by performing a surrogate analysis. Within each permutation, we randomly shuffled the pre-ERZ windows and performed the same pipeline as in the empirical data. This generated one surrogate coefficient value. The permutation was repeated 500 times and we obtained 500 surrogate coefficient values. If the circular-linear correlation coefficient derived from the empirical data exceeded the 95th percentile of the surrogate coefficient distribution, the empirical correlation value was considered significant, indicating the existence of PPLEs.

Code availability: The custom-written Matlab and Python code supporting the findings of this study will be made available upon publication.

Author contributions: L.L.Y., H.Z., and S.W. designed the research. V.N. and S.W. provided resources. L.L.Y. and K.L. performed behavior experiments. L.L.Y., H.Y.Y and H.Z. analyzed data. L.L.Y. and X.F.Y. made figure and tables. L.L.Y. and H.Z. wrote the manuscript, with comments from co-authors. H.Z. provided overall supervision. L.L.Y., S.W. and H.Z. acquired funding.

Acknowledgments: We are grateful to the patients for participating in our study. We thank the EEG technologists and nurses for assisting with data transfer and care of affected individuals during the EEG recording. This work was supported by the National Natural Science Foundation of China (81901319, 81971207 and 82171437) and DFG of Germany (ZH822/1-1).

Competing interests: The authors declare no competing interests.

Reference

Akkad, H., Dupont-Hadwen, J., Kane, E., Evans, C., Barrett, L., Frese, A., Tetkovic, I., Bestmann, S., & Stagg, C. J. (2021). Increasing human motor skill acquisition by driving theta-gamma coupling. *Elife*, *10*. https://doi.org/10.7554/eLife.67355

Allman, J. M., Watson, K. K., Tetreault, N. A., & Hakeem, A. Y. (2005). Intuition and autism: a possible role for Von Economo neurons. *Trends Cogn Sci*, *9*(8), 367-373. https://doi.org/10.1016/j.tics.2005.06.008

Apaydın, N., Üstün, S., Kale, E. H., Çelikağ, İ., Özgüven, H. D., Baskak, B., & Çiçek, M. (2018). Neural Mechanisms Underlying Time Perception and Reward Anticipation. *Front Hum Neurosci*, *12*, 115. https://doi.org/10.3389/fnhum.2018.00115

Axmacher, N., Henseler, M. M., Jensen, O., Weinreich, I., Elger, C. E., & Fell, J. (2010). Cross-frequency coupling supports multi-item working memory in the human hippocampus. *Proc Natl Acad Sci U S A*, *107*(7), 3228-3233. https://doi.org/10.1073/pnas.0911531107

Bahramisharif, A., Jensen, O., Jacobs, J., & Lisman, J. (2018). Serial representation of items during working memory maintenance at letter-selective cortical sites. *PLoS Biol*, *16*(8), e2003805. https://doi.org/10.1371/journal.pbio.2003805

Baruni, J. K., Lau, B., & Salzman, C. D. (2015). Reward expectation differentially modulates attentional behavior and activity in visual area V4. *Nat Neurosci*, *18*(11), 1656-1663. https://doi.org/10.1038/nn.4141

Bein, O., Gasser, C., Amer, T., Maril, A., & Davachi, L. (2023). Predictions transform memories: How expected versus unexpected events are integrated or separated in memory. *Neurosci Biobehav Rev*, *153*, 105368. https://doi.org/10.1016/j.neubiorev.2023.105368

Belitski, A., Gretton, A., Magri, C., Murayama, Y., Montemurro, M. A., Logothetis, N. K., & Panzeri, S. (2008). Low-frequency local field potentials and spikes in primary visual cortex convey independent visual information. *J Neurosci*, *28*(22), 5696-5709. https://doi.org/10.1523/jneurosci.0009-08.2008

Bergmann, N., Koch, D., & Schubö, A. (2019). Reward expectation facilitates context learning and attentional guidance in visual search. *J Vis*, *19*(3), 10. https://doi.org/10.1167/19.3.10

Blaukopf, C. L., & DiGirolamo, G. J. (2007). Reward, context, and human behaviour. *ScientificWorldJournal*, *7*, 626-640. https://doi.org/10.1100/tsw.2007.122

Bohbot, V. D., Copara, M. S., Gotman, J., & Ekstrom, A. D. (2017). Low-frequency theta oscillations in the human hippocampus during real-world and virtual navigation. *Nat Commun*, *8*, 14415. https://doi.org/10.1038/ncomms14415

Bush, D., & Burgess, N. (2020). Advantages and detection of phase coding in the absence of rhythmicity. *Hippocampus*, *30*(7), 745-762. https://doi.org/10.1002/hipo.23199

Cai, W., Chen, T., Ryali, S., Kochalka, J., Li, C. S., & Menon, V. (2016). Causal Interactions Within a Frontal-Cingulate-Parietal Network During Cognitive Control: Convergent Evidence from a Multisite-Multitask Investigation. *Cereb Cortex*, *26*(5), 2140-2153. https://doi.org/10.1093/cercor/bhv046

Canolty, R. T., Edwards, E., Dalal, S. S., Soltani, M., Nagarajan, S. S., Kirsch, H. E., Berger, M. S., Barbaro, N. M., & Knight, R. T. (2006). High gamma power is phase-locked to theta oscillations in human neocortex. *Science*, *313*(5793), 1626-1628. https://doi.org/10.1126/science.1128115

Canolty, R. T., & Knight, R. T. (2010). The functional role of cross-frequency coupling. *Trends Cogn Sci*, *14*(11), 506-515. https://doi.org/10.1016/j.tics.2010.09.001

Chen, C., Wang, Y., Ye, L., Xu, J., Ming, W., Liu, X., Hu, L., Ye, H., Xu, C., Wang, Y., Wang, Z., Ding, Y., Zhu, J., Ding, M., Chen, Z., & Wang, S. (2023). A region-specific modulation of sleep slow waves on interictal epilepsy markers in focal epilepsy. *Epilepsia*, *64*(4), 973-985. https://doi.org/10.1111/epi.17518

Dajani, D. R., & Uddin, L. Q. (2015). Demystifying cognitive flexibility: Implications for clinical and developmental neuroscience. *Trends Neurosci*, *38*(9), 571-578. https://doi.org/10.1016/j.tins.2015.07.003

Das, A., Myers, J., Mathura, R., Shofty, B., Metzger, B. A., Bijanki, K., Wu, C., Jacobs, J., & Sheth, S. A. (2022). Spontaneous neuronal oscillations in the human insula are hierarchically organized traveling waves. *Elife*, *11*. https://doi.org/10.7554/eLife.76702

Delorme, A., & Makeig, S. (2004). EEGLAB: an open source toolbox for analysis of single-trial EEG dynamics including independent component analysis. *J Neurosci Methods*, *134*(1), 9-21. https://doi.org/10.1016/j.jneumeth.2003.10.009

Epstein, J. N., Langberg, J. M., Rosen, P. J., Graham, A., Narad, M. E., Antonini, T. N., Brinkman, W. B., Froehlich, T., Simon, J. O., & Altaye, M. (2011). Evidence for higher reaction time variability for

children with ADHD on a range of cognitive tasks including reward and event rate manipulations. *Neuropsychology*, *25*(4), 427-441. https://doi.org/10.1037/a0022155

Faillenot, I., Heckemann, R. A., Frot, M., & Hammers, A. (2017). Macroanatomy and 3D probabilistic atlas of the human insula. *Neuroimage*, *150*, 88-98. https://doi.org/10.1016/j.neuroimage.2017.01.073

Fathy, Y. Y., Hepp, D. H., de Jong, F. J., Geurts, J. J. G., Foncke, E. M. J., Berendse, H. W., van de Berg, W. D. J., & Schoonheim, M. M. (2020). Anterior insular network disconnection and cognitive impairment in Parkinson's disease. *Neuroimage Clin*, *28*, 102364. https://doi.org/10.1016/j.nicl.2020.102364

Freunberger, R., Werkle-Bergner, M., Griesmayr, B., Lindenberger, U., & Klimesch, W. (2011). Brain oscillatory correlates of working memory constraints. *Brain Res*, *1375*, 93-102. https://doi.org/10.1016/j.brainres.2010.12.048

Frömer, R., Lin, H., Dean Wolf, C. K., Inzlicht, M., & Shenhav, A. (2021). Expectations of reward and efficacy guide cognitive control allocation. *Nat Commun*, *12*(1), 1030. https://doi.org/10.1038/s41467-021-21315-z

González, J., Cavelli, M., Mondino, A., Rubido, N., Bl Tort, A., & Torterolo, P. (2020). Communication Through Coherence by Means of Cross-frequency Coupling. *Neuroscience*, *449*, 157-164. https://doi.org/10.1016/j.neuroscience.2020.09.019

Grill-Spector, K., Henson, R., & Martin, A. (2006). Repetition and the brain: neural models of stimulus-specific effects. *Trends Cogn Sci*, *10*(1), 14-23. https://doi.org/10.1016/j.tics.2005.11.006

Hafting, T., Fyhn, M., Bonnevie, T., Moser, M. B., & Moser, E. I. (2008). Hippocampus-independent phase precession in entorhinal grid cells. *Nature*, *453*(7199), 1248-1252. https://doi.org/10.1038/nature06957

Hermoso-Mendizabal, A., Hyafil, A., Rueda-Orozco, P. E., Jaramillo, S., Robbe, D., & de la Rocha, J. (2020). Response outcomes gate the impact of expectations on perceptual decisions. *Nat Commun*, *11*(1), 1057. https://doi.org/10.1038/s41467-020-14824-w

Heusser, A. C., Poeppel, D., Ezzyat, Y., & Davachi, L. (2016). Episodic sequence memory is supported by a theta-gamma phase code. *Nat Neurosci*, *19*(10), 1374-1380. https://doi.org/10.1038/nn.4374

Hurd, Y. L., Suzuki, M., & Sedvall, G. C. (2001). D1 and D2 dopamine receptor mRNA expression in whole hemisphere sections of the human brain. *J Chem Neuroanat*, *22*(1-2), 127-137. https://doi.org/10.1016/s0891-0618(01)00122-3

Jones, M. W., & Wilson, M. A. (2005). Phase precession of medial prefrontal cortical activity relative to the hippocampal theta rhythm. *Hippocampus*, *15*(7), 867-873. https://doi.org/10.1002/hipo.20119

Kahana, M. J., Sekuler, R., Caplan, J. B., Kirschen, M., & Madsen, J. R. (1999). Human theta oscillations exhibit task dependence during virtual maze navigation. *Nature*, *399*(6738), 781-784. https://doi.org/10.1038/21645

Kok, P., Failing, M. F., & de Lange, F. P. (2014). Prior expectations evoke stimulus templates in the primary visual cortex. *J Cogn Neurosci*, *26*(7), 1546-1554. https://doi.org/10.1162/jocn_a_00562

Kragel, J. E., VanHaerents, S., Templer, J. W., Schuele, S., Rosenow, J. M., Nilakantan, A. S., & Bridge, D. J. (2020). Hippocampal theta coordinates memory processing during visual exploration. *Elife*, *9*. https://doi.org/10.7554/eLife.52108

Kriegeskorte, N., Mur, M., & Bandettini, P. (2008). Representational similarity analysis - connecting the branches of systems neuroscience. *Front Syst Neurosci*, *2*, 4. https://doi.org/10.3389/neuro.06.004.2008

Kurth, F., Zilles, K., Fox, P. T., Laird, A. R., & Eickhoff, S. B. (2010). A link between the systems: functional differentiation and integration within the human insula revealed by meta-analysis. *Brain Struct Funct*, *214*(5-6), 519-534. https://doi.org/10.1007/s00429-010-0255-z

Lansink, C. S., Meijer, G. T., Lankelma, J. V., Vinck, M. A., Jackson, J. C., & Pennartz, C. M. (2016). Reward Expectancy Strengthens CA1 Theta and Beta Band Synchronization and Hippocampal-Ventral Striatal Coupling. *J Neurosci*, *36*(41), 10598-10610. https://doi.org/10.1523/jneurosci.0682-16.2016

Lehongre, K., Lambrecq, V., Whitmarsh, S., Frazzini, V., Cousyn, L., Soleil, D., Fernandez-Vidal, S., Mathon, B., Houot, M., Lemaréchal, J. D., Clemenceau, S., Hasboun, D., Adam, C., & Navarro, V. (2022). Long-term deep intracerebral microelectrode recordings in patients with drug-resistant epilepsy: Proposed guidelines based on 10-year experience. *Neuroimage*, *254*, 119116. https://doi.org/10.1016/j.neuroimage.2022.119116

Lisman, J. (2005). The theta/gamma discrete phase code occuring during the hippocampal phase precession may be a more general brain coding scheme. *Hippocampus*, *15*(7), 913-922. https://doi.org/10.1002/hipo.20121

Lisman, J. E., & Idiart, M. A. (1995). Storage of 7 +/- 2 short-term memories in oscillatory subcycles. *Science*, *267*(5203), 1512-1515. https://doi.org/10.1126/science.7878473

Lopes-Dos-Santos, V., van de Ven, G. M., Morley, A., Trouche, S., Campo-Urriza, N., & Dupret, D. (2018). Parsing Hippocampal Theta Oscillations by Nested Spectral Components during Spatial Exploration and Memory-Guided Behavior. *Neuron*, *100*(4), 940-952.e947. https://doi.org/10.1016/j.neuron.2018.09.031

Lopour, B. A., Tavassoli, A., Fried, I., & Ringach, D. L. (2013). Coding of information in the phase of local field potentials within human medial temporal lobe. *Neuron*, *79*(3), 594-606. https://doi.org/10.1016/j.neuron.2013.06.001

Mariscal, M. G., Berry-Kravis, E., Buxbaum, J. D., Ethridge, L. E., Filip-Dhima, R., Foss-Feig, J. H., Kolevzon, A., Modi, M. E., Mosconi, M. W., Nelson, C. A., Powell, C. M., Siper, P. M., Soorya, L., Thaliath, A., Thurm, A., Zhang, B., Sahin, M., & Levin, A. R. (2021). Shifted phase of EEG cross-frequency coupling in individuals with Phelan-McDermid syndrome. *Mol Autism*, *12*(1), 29. https://doi.org/10.1186/s13229-020-00411-9

Mariscal, M. G., Levin, A. R., Gabard-Durnam, L. J., Xie, W., Tager-Flusberg, H., & Nelson, C. A. (2021). EEG Phase-Amplitude Coupling Strength and Phase Preference: Association with Age over the First Three Years after Birth. *eNeuro*, *8*(3). https://doi.org/10.1523/eneuro.0264-20.2021

McGinn, R. J., & Valiante, T. A. (2014). Phase-amplitude coupling and interlaminar synchrony are correlated in human neocortex. *J Neurosci*, *34*(48), 15923-15930. https://doi.org/10.1523/jneurosci.2771-14.2014

Mesulam, M. M., & Mufson, E. J. (1982). Insula of the old world monkey. III: Efferent cortical output and comments on function. *J Comp Neurol*, *212*(1), 38-52. https://doi.org/10.1002/cne.902120104

Mizuhiki, T., Richmond, B. J., & Shidara, M. (2012). Encoding of reward expectation by monkey anterior insular neurons. *J Neurophysiol*, *107*(11), 2996-3007. https://doi.org/10.1152/jn.00282.2011

Molnar-Szakacs, I., & Uddin, L. Q. (2022). Anterior insula as a gatekeeper of executive control. *Neurosci Biobehav Rev*, *139*, 104736. https://doi.org/10.1016/j.neubiorev.2022.104736

O'Doherty, J. P., Deichmann, R., Critchley, H. D., & Dolan, R. J. (2002). Neural responses during anticipation of a primary taste reward. *Neuron*, *33*(5), 815-826. https://doi.org/10.1016/s0896-6273(02)00603-7

O'Keefe, J., & Recce, M. L. (1993). Phase relationship between hippocampal place units and the EEG theta rhythm. *Hippocampus*, *3*(3), 317-330. https://doi.org/10.1002/hipo.450030307

Özkurt, T. E., & Schnitzler, A. (2011). A critical note on the definition of phase-amplitude cross-frequency coupling. *J Neurosci Methods*, *201*(2), 438-443. https://doi.org/10.1016/j.jneumeth.2011.08.014

Pessiglione, M., Schmidt, L., Draganski, B., Kalisch, R., Lau, H., Dolan, R. J., & Frith, C. D. (2007). How the brain translates money into force: a neuroimaging study of subliminal motivation. *Science*, *316*(5826), 904-906. https://doi.org/10.1126/science.1140459

Qasim, S. E., Fried, I., & Jacobs, J. (2021). Phase precession in the human hippocampus and entorhinal cortex. *Cell*, *184*(12), 3242-3255.e3210. https://doi.org/10.1016/j.cell.2021.04.017

Ray, S., & Maunsell, J. H. (2011). Different origins of gamma rhythm and high-gamma activity in macaque visual cortex. *PLoS Biol*, *9*(4), e1000610. https://doi.org/10.1371/journal.pbio.1000610

Rayan, A., Donoso, J. R., Mendez-Couz, M., Dolón, L., Cheng, S., & Manahan-Vaughan, D. (2022). Learning shifts the preferred theta phase of gamma oscillations in CA1. *Hippocampus*, *32*(9), 695-704. https://doi.org/10.1002/hipo.23460

Reddy, L., Self, M. W., Zoefel, B., Poncet, M., Possel, J. K., Peters, J. C., Baayen, J. C., Idema, S., VanRullen, R., & Roelfsema, P. R. (2021). Theta-phase dependent neuronal coding during sequence learning in human single neurons. *Nat Commun*, *12*(1), 4839. https://doi.org/10.1038/s41467-021-25150-0

Reifenstein, E. T., Bin Khalid, I., & Kempter, R. (2021). Synaptic learning rules for sequence learning. *Elife*, *10*. https://doi.org/10.7554/eLife.67171

Rothkirch, M., Schmack, K., Deserno, L., Darmohray, D., & Sterzer, P. (2014). Attentional modulation of reward processing in the human brain. *Hum Brain Mapp*, *35*(7), 3036-3051. https://doi.org/10.1002/hbm.22383

Rowe, J. B., Eckstein, D., Braver, T., & Owen, A. M. (2008). How does reward expectation influence cognition in the human brain? *J Cogn Neurosci*, *20*(11), 1980-1992. https://doi.org/10.1162/jocn.2008.20140

Schneider, M., Leuchs, L., Czisch, M., Sämann, P. G., & Spoormaker, V. I. (2018). Disentangling reward anticipation with simultaneous pupillometry / fMRI. *Neuroimage*, *178*, 11-22. https://doi.org/10.1016/j.neuroimage.2018.04.078

Seeley, W. W., Menon, V., Schatzberg, A. F., Keller, J., Glover, G. H., Kenna, H., Reiss, A. L., & Greicius, M. D. (2007). Dissociable intrinsic connectivity networks for salience processing and executive control. *J Neurosci*, *27*(9), 2349-2356. https://doi.org/10.1523/jneurosci.5587-06.2007

Seymour, R. A., Rippon, G., & Kessler, K. (2017). The Detection of Phase Amplitude Coupling during Sensory Processing. *Front Neurosci*, *11*, 487. https://doi.org/10.3389/fnins.2017.00487

Siegel, M., Warden, M. R., & Miller, E. K. (2009). Phase-dependent neuronal coding of objects in short-term memory. *Proc Natl Acad Sci U S A*, *106*(50), 21341-21346. https://doi.org/10.1073/pnas.0908193106

Skaggs, W. E., McNaughton, B. L., Wilson, M. A., & Barnes, C. A. (1996). Theta phase precession in hippocampal neuronal populations and the compression of temporal sequences. *Hippocampus*, *6*(2), 149-172. https://doi.org/10.1002/(sici)1098-1063(1996)6:2<149::Aid-hipo6>3.0.Co;2-k

Speers, L. J., Schmidt, R., & Bilkey, D. K. (2022). Aberrant Phase Precession of Lateral Septal Cells in a Maternal Immune Activation Model of Schizophrenia Risk May Disrupt the Integration of Location with Reward. *J Neurosci*, *42*(20), 4187-4201. https://doi.org/10.1523/jneurosci.0039-22.2022

Sridharan, D., Levitin, D. J., & Menon, V. (2008). A critical role for the right fronto-insular cortex in switching between central-executive and default-mode networks. *Proc Natl Acad Sci U S A*, *105*(34), 12569-12574. https://doi.org/10.1073/pnas.0800005105

Sun, K., Xiao, L., Wu, Y., Zuo, D., Zhang, C., Liu, S., He, Z., Rong, S., Wang, F., & Sun, T. (2020). GABAergic neurons in the insular cortex play an important role in cue-morphine reward memory reconsolidation. *Life Sci*, *254*, 117655. https://doi.org/10.1016/j.lfs.2020.117655

Tingley, D., & Buzsáki, G. (2018). Transformation of a Spatial Map across the Hippocampal-Lateral Septal Circuit. *Neuron*, *98*(6), 1229-1242.e1225. https://doi.org/10.1016/j.neuron.2018.04.028

Tort, A. B., Komorowski, R. W., Manns, J. R., Kopell, N. J., & Eichenbaum, H. (2009). Theta-gamma coupling increases during the learning of item-context associations. *Proc Natl Acad Sci U S A*, *106*(49), 20942-20947. https://doi.org/10.1073/pnas.0911331106

Uddin, L. Q., Kinnison, J., Pessoa, L., & Anderson, M. L. (2014). Beyond the tripartite cognition-emotion-interoception model of the human insular cortex. *J Cogn Neurosci*, *26*(1), 16-27. https://doi.org/10.1162/jocn_a_00462

van der Meer, M. A., & Redish, A. D. (2011). Theta phase precession in rat ventral striatum links place and reward information. *J Neurosci*, *31*(8), 2843-2854. https://doi.org/10.1523/jneurosci.4869-10.2011

Watrous, A. J., Deuker, L., Fell, J., & Axmacher, N. (2015). Phase-amplitude coupling supports phase coding in human ECoG. *Elife*, *4*. https://doi.org/10.7554/eLife.07886

Watrous, A. J., Miller, J., Qasim, S. E., Fried, I., & Jacobs, J. (2018). Phase-tuned neuronal firing encodes human contextual representations for navigational goals. *Elife*, *7*. https://doi.org/10.7554/eLife.32554

Xue, G., Dong, Q., Chen, C., Lu, Z., Mumford, J. A., & Poldrack, R. A. (2010). Greater neural pattern similarity across repetitions is associated with better memory. *Science*, *330*(6000), 97-101. https://doi.org/10.1126/science.1193125

Yang, A. I., Dikecligil, G. N., Jiang, H., Das, S. R., Stein, J. M., Schuele, S. U., Rosenow, J. M., Davis, K. A., Lucas, T. H., & Gottfried, J. A. (2021). The what and when of olfactory working memory in humans. *Curr Biol*, *31*(20), 4499-4511.e4498. https://doi.org/10.1016/j.cub.2021.08.004

Zhang, H. (2023). How Can I Conduct Surrogate Analyses, and How Should I Shuffle? In N. Axmacher (Ed.), *Intracranial EEG: A Guide for Cognitive Neuroscientists* (pp. 567-577). Springer International Publishing. https://doi.org/10.1007/978-3-031-20910-9_35

Zhang, H., Fell, J., & Axmacher, N. (2018). Electrophysiological mechanisms of human memory consolidation. *Nat Commun*, *9*(1), 4103. https://doi.org/10.1038/s41467-018-06553-y

Zhang, H., Fell, J., Staresina, B. P., Weber, B., Elger, C. E., & Axmacher, N. (2015). Gamma power reductions accompany stimulus-specific representations of dynamic events. *Curr Biol*, *25*(5), 635-640. https://doi.org/10.1016/j.cub.2015.01.011

Zheng, J., Skelin, I., & Lin, J. J. (2022). Neural computations underlying contextual processing in humans. *Cell Rep*, *40*(12), 111395. https://doi.org/10.1016/j.celrep.2022.111395

Graphic abstract

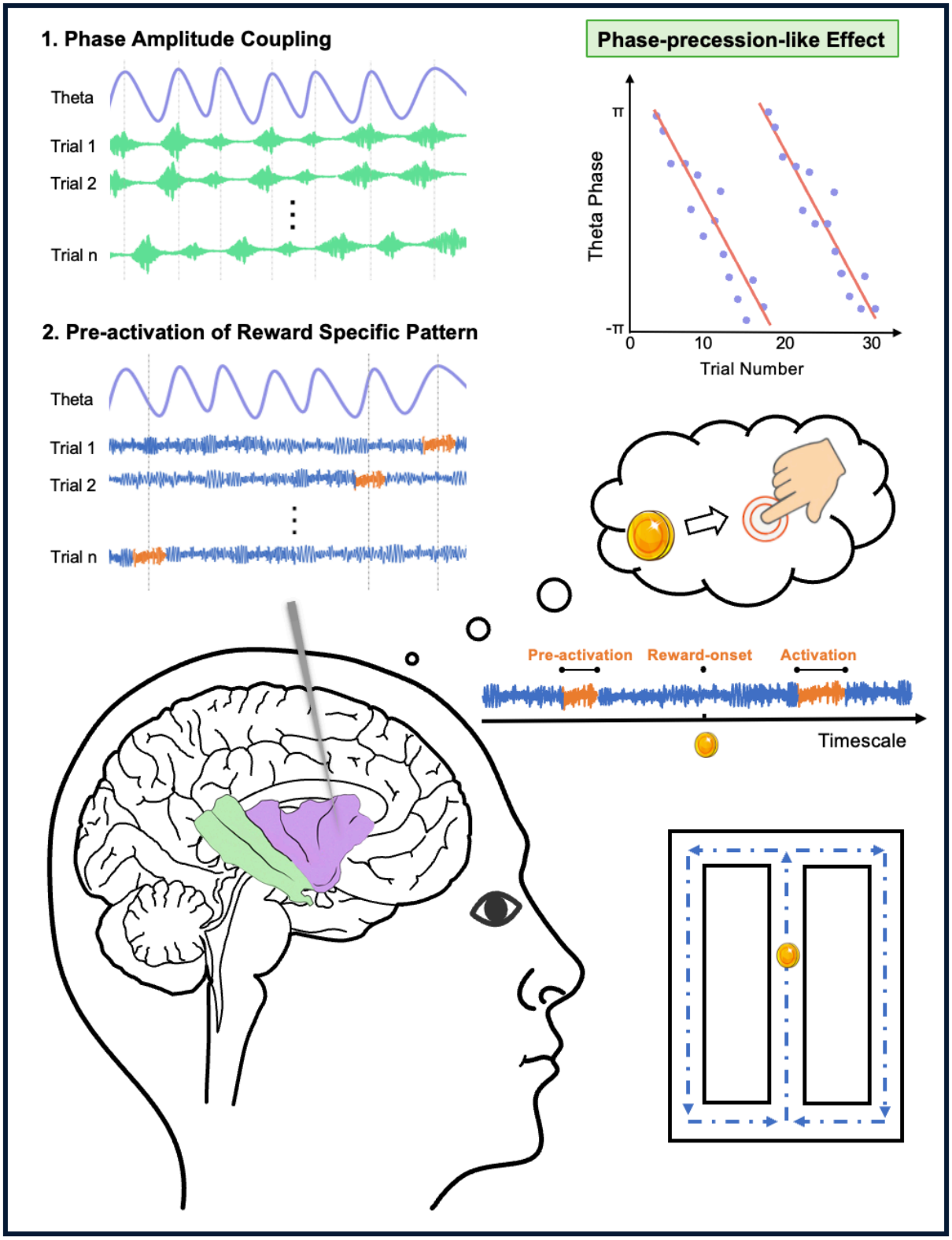

Figure legend

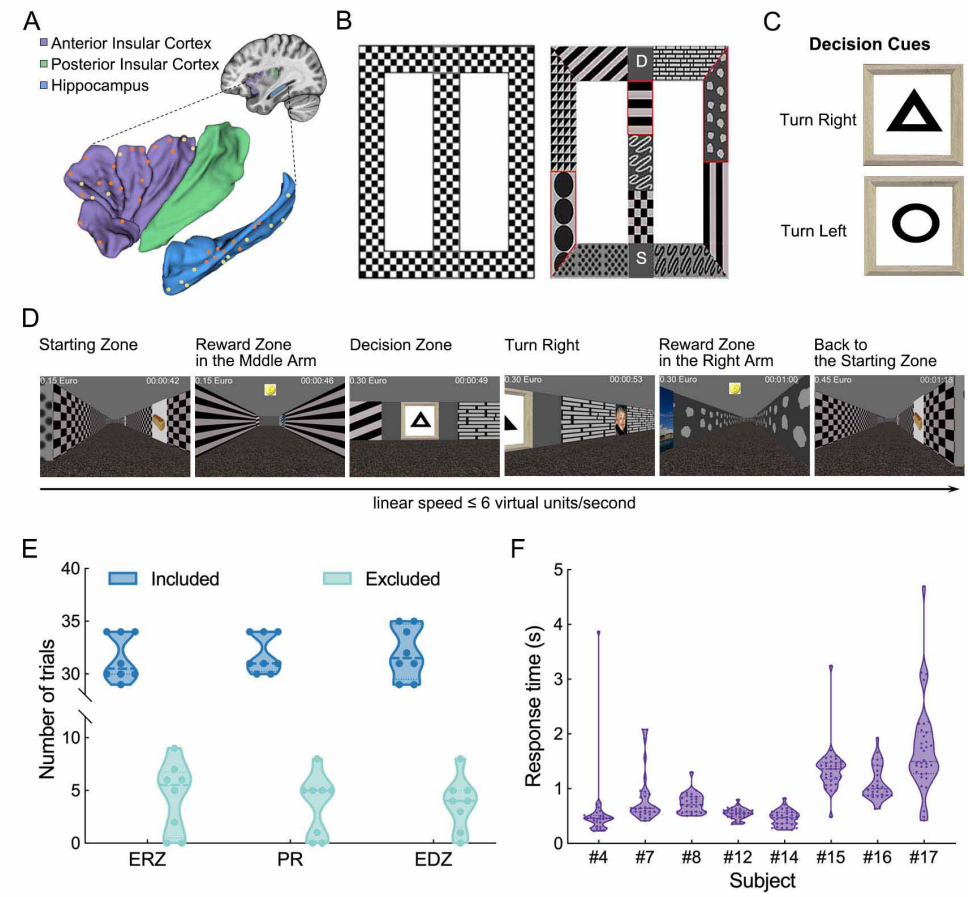

Figure 1. Contact locations, experimental paradigm and behavioral performance.

(A) Spatial distribution of contacts in the anterior insular cortex (AIC, purple), posterior insular cortex (PIC, green), and hippocampus (HPC, blue). For illustration purposes, contacts from both hemispheres are drawn together. Each orange sphere indicates a contact in the right hemisphere, and each yellow sphere indicates a contact in the left hemisphere. **(B)** Overhead view of the T maze. Left panel: Diagram of the virtual maze. Each small square represents one square virtual unit. Right panel: The T maze adorned with various patterns on its walls. The gray square marked with "S" represents the starting zone where each trial starts and ends, while the gray square marked with "D" represents the decision zone where subjects are expected to choose the correct direction according to the cue. The areas circled with red lines represent the reward zones, where subjects are expected to collect gold coins by pressing the Enter button as soon as possible. Otherwise, the reward disappears when they are outside of the reward zone. **(C)** Cues on the wall of the decision zone. Circle represents turning left and triangle represents turning right (counterbalanced across subjects). **(D)** An example trial from the first-person perspective in the maze. **(E)** Included (blue) and excluded (green) trials are similar across conditions. Note that there is a discontinuity in the y-axis to enhance visualization. ERZ: entering the reward zone; PZ: picking up the reward; EDZ: entering the decision zone. Each dot within violin plots indicates a subject. **(F)** Behavioral performance for subjects with AIC contacts. Each violin plot indicates a subject, and each dot within violin plots indicates a trial.

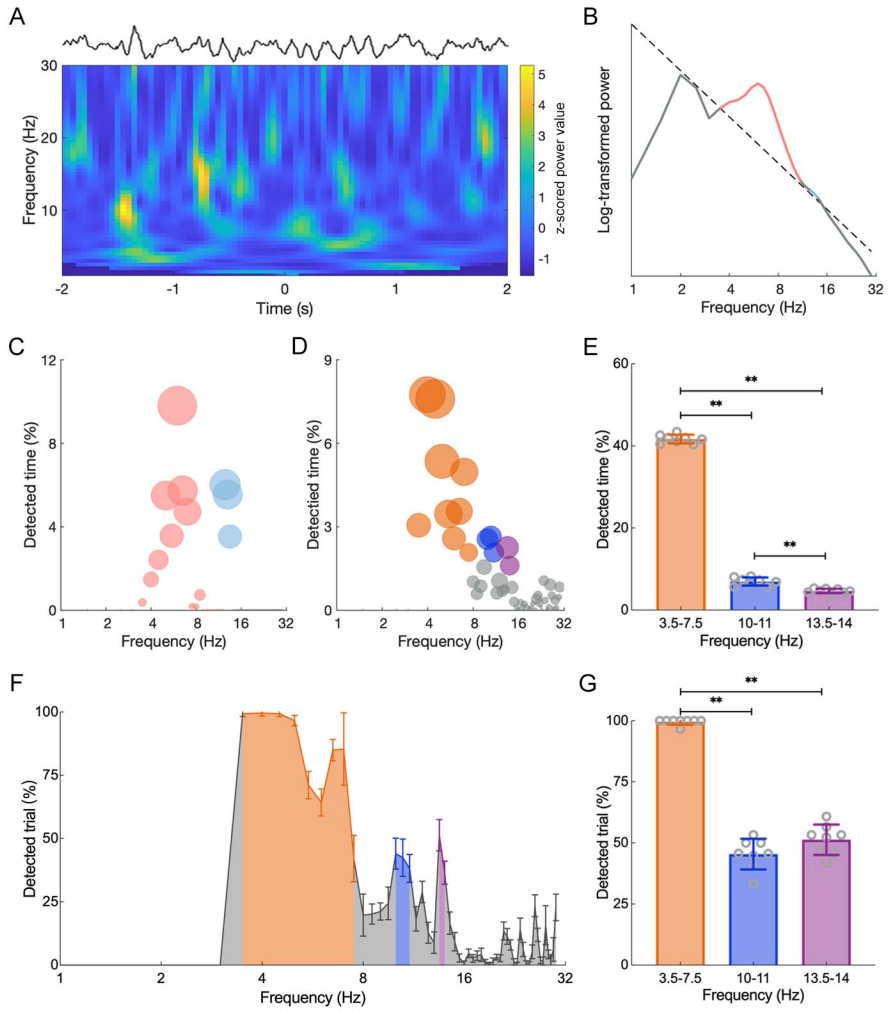

Figure 2. Low-frequency oscillations detected in the AIC locked to entering the reward zone.

(A-C) An example trial from a contact located in the right anterior insular cortex (AIC) of subject #14. **(A)** Raw trace and its time-frequency spectrum in the example trial. Zero represents the timepoint of entering the reward zone. **(B)** Two narrow-band oscillations (3.5-11Hz indicated by the solid pink line; 12.5-14Hz indicated by the solid light blue line) are identified as contiguous frequencies exceeding the fitted line using MODAL (Watrous et al., 2018). **(C)** Prevalence of oscillations at each frequency from trial shown in panel **(B)**. The larger the sphere, the higher the percentage of detected time of the corresponding frequency. **(D-G)** Population data for all AIC contacts demonstrating three low frequency oscillations represented by three different colors. Orange indicates 3.5-7.5Hz, dark blue indicates 10-11Hz, purple indicates 13.5-14Hz, and grey indicates frequencies that did not exceed the fitted line in MODAL. **(D)** Percentage of time periods during which oscillatory activities are detected separately for each frequency. **(E)** Proportion of time periods for each detected oscillation band. Gray rings indicate individual subject. Error bars indicate one standard deviation (SD) from the mean, and ** is corresponding to $0.005 \leqslant p < 0.01$. **(F)** Proportion of trials with detected oscillations at each frequency. Error bars indicate one SD from the mean. **(G)** Proportion of trials in which oscillations are detected in each identified frequency band. Gray rings indicate individual contacts, error bars indicate one SD from the mean, and ** indicates $0.005 \leqslant p < 0.01$.

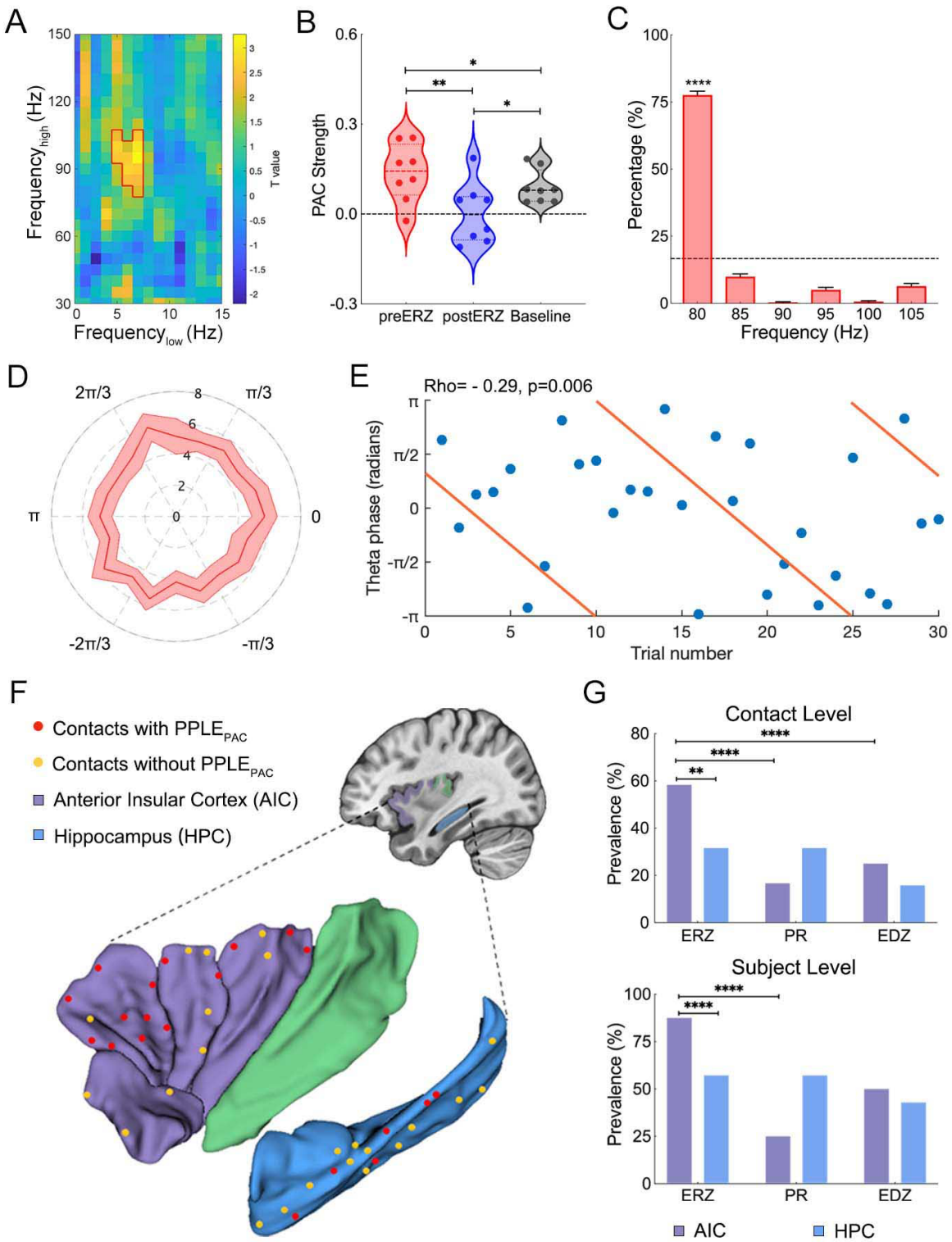

Figure 3. PAC and PPLE$_{PAC}$ before entering reward zones in the AIC.

(A) Differences in phase-amplitude coupling (PAC) between pre- and post-ERZ events. The frequency$_{low}$-frequency$_{high}$ cluster circled in red lines shows enhanced PAC effects for pre-ERZ events than post-ERZ events (Frequency$_{low}$: 5-7Hz; frequency$_{high}$: 80-105Hz). **(B)** Average PAC value within the frequency$_{low}$-frequency$_{high}$ cluster from panel A for individual subjects in pre-ERZ, post-ERZ, and baseline conditions.

Each dot indicates one subject. *: $0.01 \leq p < 0.05$, **: $0.005 \leq p < 0.01$. **(C)** Probability density of the peak gamma frequency of the PAC effect. The dashed line indicates the probability density of the even distribution (16.67%), the error bar indicates one SEM. ****: $p<0.001$. (**D)** Distribution of theta phases corresponding to the peak gamma power. The red line indicates the average probability density over contacts, the shaded area indicates one SEM from the mean. **(E)** An example showing that the peak of gamma power is locked to earlier theta phases over trials when subjects are approaching the same reward zone. Blue spheres indicate individual trials and the orange lines indicate the fitted line between theta phases corresponding to peak gamma power and trial numbers. **(F)** Spatial distribution of contacts showing $PPLE_{PAC}$ in the AIC (anterior insular cortex) and HPC (the hippocampus). **(G)** Prevalence of $PPLE_{PAC}$ in the AIC and HPC for each condition at contact (upper panel) and subject (lower panel) levels. ERZ: entering the reward zone; PR: picking up the reward; EDZ: entering the decision zones. **: $0.005 \leq p < 0.01$; ****: $p<0.001$.

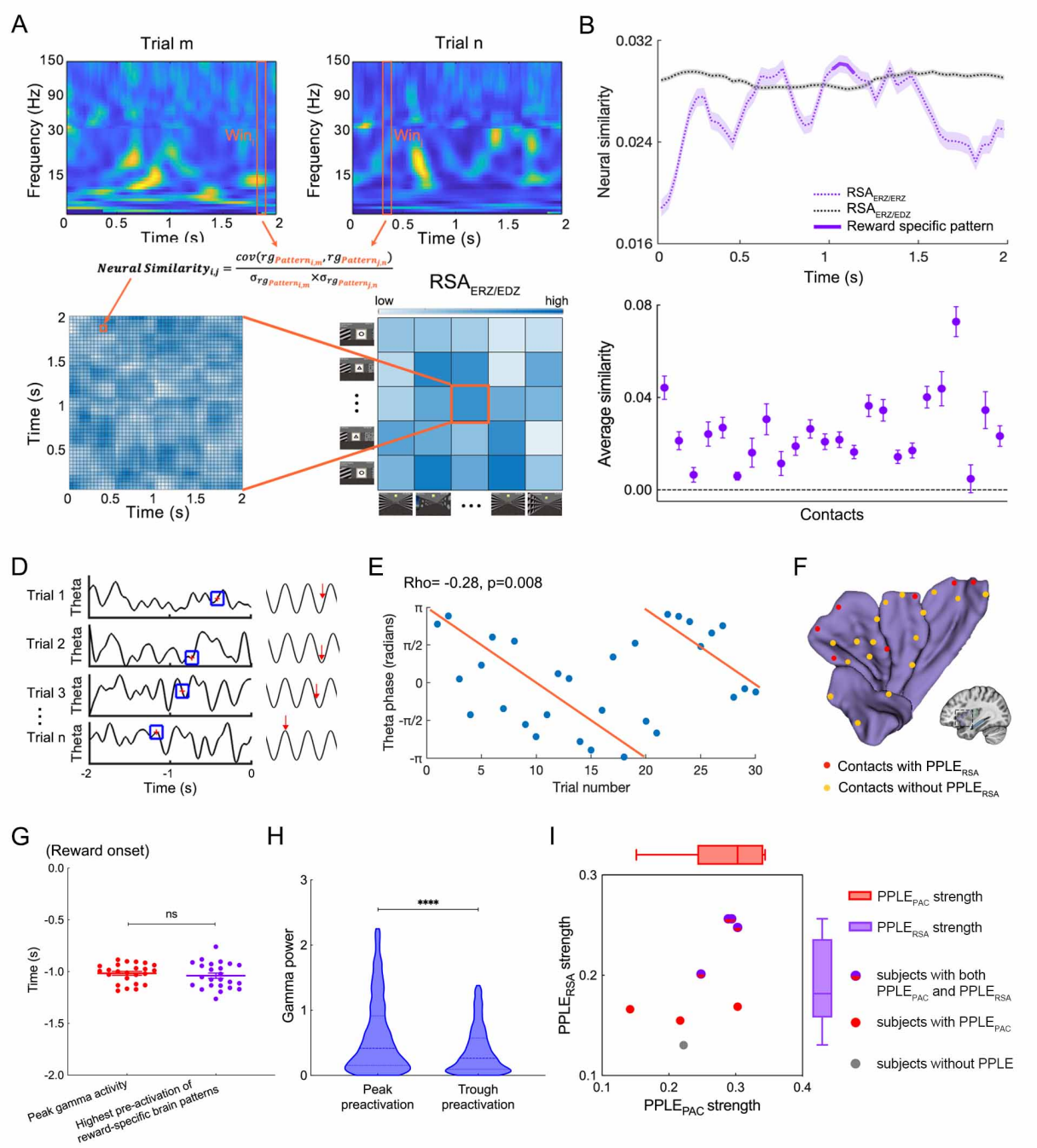

Figure 4. Pre-activation of reward-specific brain patterns and $PPLE_{RSA}$ before entering reward zones in the AIC.

(A) Scheme of representational similarity analysis (RSA) for extracting reward-specific representations. We calculated the similarity of neural patterns between any two post-ERZ events at different locations (Figure 1B; $RSA_{ERZ/ERZ}$), as well as between post-ERZ and post-EDZ events ($RSA_{ERZ/EDZ}$). ERZ: entering the reward zone; EDZ: entering the decision zone. **(B)** Time courses of neural similarities of post-ERZ/post-ERZ periods ($RSA_{ERZ/ERZ}$, indicated by the purple dashed line) and post-EDZ/post-ERZ periods ($RSA_{ERZ/EDZ}$, indicated by the black dashed line). X axis indicates the time course of post-ERZ period, 0

indicates onset of rewards, and shaded area indicates SEM. The solid lines represent the time windows of reward-specific patterns, in which $RSA_{ERZ/ERZ}$ values are significantly greater than $RSA_{ERZ/EDZ}$ values. **(C)** Reward-specific brain patterns are pre-activated before the onset of reward showing that brain patterns during pre-ERZ periods are similar to reward-specific representations. Each sphere indicates one channel, error bar indicates one SEM. **(D)** An illustration of the $PPLE_{RSA}$. Theta phases, in which the reward-specific patterns are pre-activated, progressively shift forward across successive trials of a given AIC contact. Each red '+' inside the blue box and the red arrow on the left panel indicate the theta phases of the peak pre-activation time. Time 0 indicates the onset of the reward. **(E)** An example of a contact exhibiting $PPLE_{RSA}$. Pre-activation of the reward-specific brain patterns is locked to progressively earlier theta phases over trials, indicating $PPLE_{RSA}$. Each blue sphere indicates one trial. Orange lines indicate the fitted line between trial numbers and theta phases to which the peak pre-activation of reward-specific brain patterns is locked. **(F)** Distribution of contacts exhibiting $PPLE_{RSA}$ in the AIC. **(G)** Peak gamma activities showing PAC effects and the highest pre-activation of reward specific brain patterns tend to occur at similar time. Each red sphere indicates the timepoint of peak gamma activity, each purple sphere indicates the timepoint of the pre-activation of reward specific brain patterns. Y axis indicates the time course of pre-ERZ period, time 0 indicates onset of rewards. Error bar indicates one SEM. ns, no significant difference. **(H)** The difference in gamma power between the timepoints corresponding to the peak and trough pre-activation of reward-specific brain patterns. ****, $p<0.001$. **(I)** Strength of $PPLLE_{PAC}$ and $PPLE_{RSA}$ for subjects with AIC contacts. Each sphere indicates one subject. Note that the PPLE strength here represents the absolute value of coefficients extracted form circular-linear correlations shown in panel (E).

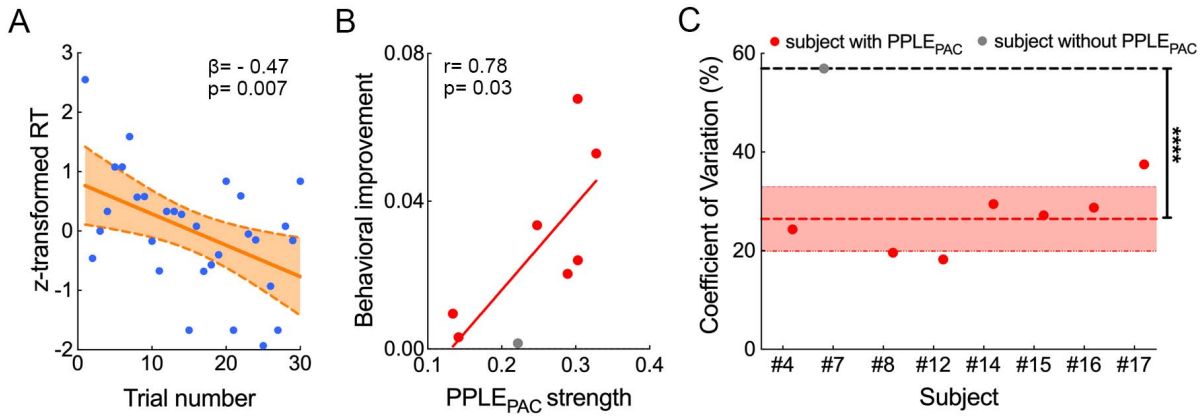

Figure 5. Functional relevance of PPLE$_{PAC}$

(A) An example showing that the response time (RT) decreases with increased trial numbers. Blue spheres indicate individual trials and the orange line indicates the fitted line between z-transformed RT and trial numbers. Shaded area represents the 95% confidence interval of the fitted line. **(B)** Behavioral performance improved faster for subjects with stronger PPLE$_{PAC}$. Red spheres indicate individual subjects exhibiting PPLE$_{PAC}$, the gray sphere indicates the subject without PPLE$_{PAC}$. Note that the behavioral improvement represents the absolute values of the slope (unstandardized coefficients) for the fitted lines as illustrated in panel (**A**) and Figure S5. **(C)** Subjects with AIC contacts showing PPLE$_{PAC}$ had significantly shorter RT variability than the subject without PPLE$_{PAC}$. Shaded areas indicate one SD from the mean. ****, $p<0.001$.